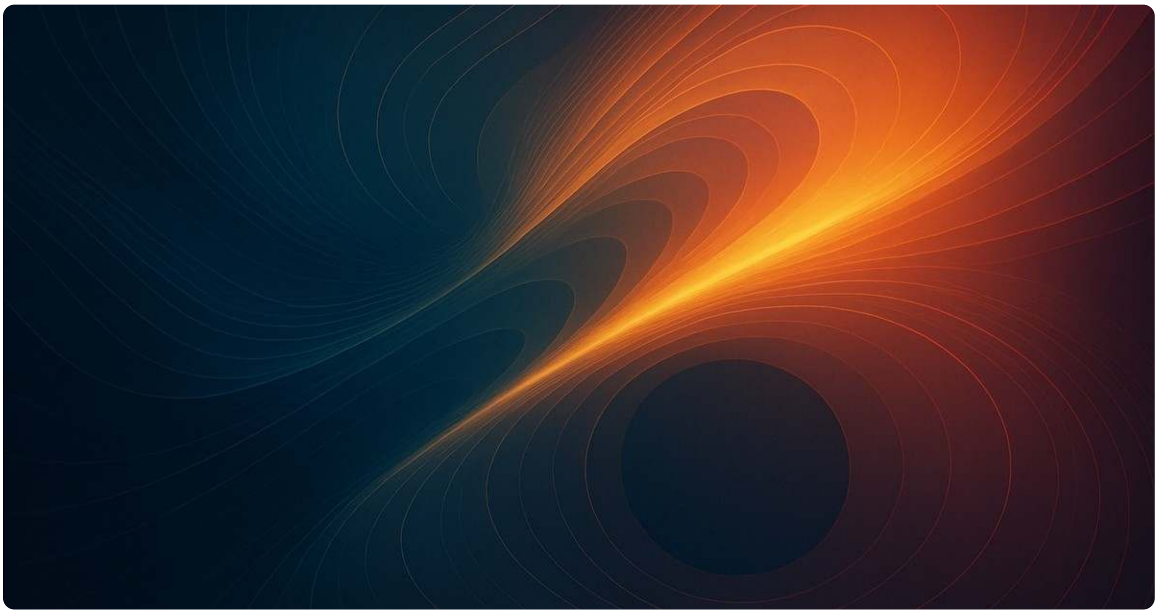

Temporal Equivalence Principle: Dynamic Time & Emergent Light Speed

Matthew Lukin Smawfield

Version: v0.13 (Jakarta)

First published: 18 August 2025 · Last updated: 15 September 2026

DOI: 10.5281/zenodo.16921911

Abstract

This paper proposes a covariant, testable reformulation of relativity in which proper time is a dynamical field and the "speed of light" is an emergent, strictly local invariant rather than a global constant. The framework is built on a single spacetime manifold endowed with two metrics: a gravitational metric $g_{\mu\nu}$ and a causal (matter) metric $\tilde{g}_{\mu\nu}$ to which all non-gravitational fields and clocks couple. The metrics are related by a controlled disformal map, $\tilde{g}_{\mu\nu} = A^2(\phi) g_{\mu\nu} + B(\phi)\nabla_\mu\phi\nabla_\nu\phi$, where ϕ is the time field, $A(\phi) = \exp(\beta_A\phi/M_{\rm Pl})$ is a universal conformal factor, and $B(\phi)$ encodes tiny, direction-dependent deformations of the light cone consistent with GW170817-class multi-messenger constraints ($|c_\gamma - c_g|/c \lesssim \mathrm{few}\times 10^{-15}$ today). Proper time is elevated to a field by postulating that all matter, electromagnetism, and quantum phases evolve with respect to $\tilde{g}$-proper time τ; in local freely falling frames, this guarantees exact local Lorentz invariance and a locally invariant c, while globally it implies that synchronization procedures and one-way light-time measurements can become path-dependent in the disformal/non-exact sector of a dynamical-time background. The covariant action, field equations, conservation laws, and PPN mapping are developed; screening is formulated as continuous Temporal Topology, with the quartic density-dependent-mass branch providing an explicit microscopic completion of the Solar-System/interstellar screening requirements. The breakdown of global simultaneity is formalized using a synchronization-transport law, deriving a convention-independent "synchronization holonomy," an invariant measure of non-integrability of time transport around closed loops. In the purely conformal subclass this holonomy vanishes after subtraction of the full GR, kinematic, clock-scale, and reference-frame synchronization model; nonzero holonomy at leading order requires residual non-exact synchronization structure, supplied in the minimal TEP model by disformal coupling $B(\phi) \neq 0$, and in more general extensions by non-metricity or other explicitly non-exact transport structure. Explicit small-B formulas are provided for the holonomy and the effective photon phase speed, showing how the measured one-way asymmetry is related to ϕ-gradients and disformal scales under current constraints. The analysis demonstrates that Einstein's assumption of a universal c was a brilliant local theorem arising from the Temporal Equivalence Principle; transcending it demands dynamical time: c remains exactly invariant locally, but global, one-way-inferred "c" values differ by path-dependent amounts that experiments can detect or bound. Cosmologically, TEP adopts an eternal, static spatial background: observed redshift and the apparent Hubble relation are reconstructed through dynamical proper-time transport, $1 + z = A_0/A_{\rm em}$, rather than physical expansion of the underlying spatial manifold. Early-universe closure is achieved natively without a Big Bang singularity or phenomenological thermal screening: the framework establishes a regular temporal horizon with an unbounded local proper-time history, while the associated conformal temporal geometry preserves the observed CMB acoustic structure. Known weaknesses in the variable-c literature are addressed by supplying a correct, operationally invariant observable (holonomy), clarifying when conformal couplings cannot produce a signal, and providing realistic, constraint-consistent benchmark sensitivity windows *with explicit error budgets and statistical plans (pre-registration, blinding, publicly released code and data). The resulting theory preserves the empirical pillars of relativity (local Lorentz invariance, gravitational-wave causality, PPN bounds) while extending its conceptual foundation: simultaneity is not only relative but generally non-integrable; the speed of light is not a global constant but the local echo of a deeper, dynamical temporal geometry.*

Long-standing confusions about "variable c*" are resolved by replacing convention-dependent statements with invariant observables tied to measurement procedures. A synchronization one-form* $\tilde{\sigma}$ *is defined on spacelike slices of the matter metric; its curl* $d\tilde{\sigma}$*, after subtraction of the full GR, kinematic, clock-scale, and reference-frame synchronization model, yields a residual "temporal holonomy"* H *that vanishes in GR and becomes nonzero only when time is dynamical in this sense. Two key theorems are proven: (i) conformal matter coupling preserves null cones, so photons and gravitons share the same causal structure at late times; (ii) a static* ϕ*-gradient produces no direct propagation asymmetry in the static purely conformal limit—the cancellation is exact, not merely first-order. Disformal tilts (*$B \neq 0$*) are tightly constrained by GW170817-class multi-messenger observations but can source holonomy at levels within reach of next-generation metrology. The effective covariant architecture is presented; field equations, conservation laws, invertibility/causality conditions, and a 3+1 decomposition are derived to make the observables explicit. Screening via a continuous Temporal Topology governed by non-linear superposition of field gradients (Temporal Shear) reconciles precision local tests with cosmological evolution, with mapping to Parametrized Post-Newtonian parameters and to the EFT-of-dark-energy* α*-functions with* $c_T = 1$ *enforced. Decisive experiments with quantitative error budgets are outlined: (1) a ground–ground–satellite triangle time-transfer experiment targeting holonomy at below* 10^{-18} *fractional after GR subtraction; (2) portable-clock "clock anholonomy" around closed paths at the* 10^{-19} *level over days; (3) multi-species clock networks seeking phase-locked annual modulations at* 10^{-19}*–*10^{-17}*; (4) interplanetary one-way optical links at picoseconds over AU; (5) altitude-dependent screening maps with optical clocks and atom interferometers; and (6) ensemble multi-messenger tests. A cosmological pipeline plan for CLASS/HyRec modifications and MCMC inference is provided, with commitment to open data and blinded analyses.*

Einstein's postulate of universal c *was a brilliant, operationally perfect approximation in regimes where time's flow is effectively uniform. In a universe where the rate of time is dynamical yet locally Lorentzian, "the speed of light" emerges as an invariant in every local lab but ceases to be globally universal. The new invariant content resides in path-dependent synchronization defects and holonomies of time transport, not in naive one-way "speeds." If detected, these invariants would inaugurate a post-Einsteinian era: from dynamic geometry to dynamic time.*

1. Introduction: From a Universal Speed to a Universal Principle of Time

Relativity and quantum theory disagree about time. General relativity (GR) makes proper time geometric—$d\tau^2 = -g_{\mu\nu}dx^\mu dx^\nu/c^2$—dynamical, and observer-dependent. Quantum mechanics (QM) treats time as an external parameter t in the Schrödinger equation, $i\hbar\partial_t|\psi\rangle = \hat{H}|\psi\rangle$. The clash has haunted quantization programs for a century and manifested operationally as subtle ambiguities in defining one-way light speeds and simultaneity across extended regions. Precision clocks and time-transfer links now measure gravitational redshifts and velocity-dependent dilations at 10^{-18} fractional levels, while cosmology exhibits persistent H_0 and S_8 tensions. In this context, Einstein's postulate of a universal speed c must be sharpened: it is exact for any local freely falling laboratory, but it cannot be a global property if the flow of time itself is dynamical.

The Temporal Equivalence Principle (TEP) is proposed: all non-gravitational dynamics, signals, and quantum phases evolve according to the proper time defined by a single causal metric $\tilde{g}_{\mu\nu}$ that couples universally to matter. The rate at which proper time accrues is a field. This elevates "when" to the status "where" acquired in 1915: as space was geometrized, now time's rate is dynamized. The consequence is that synchronization conventions can become globally non-integrable when the dynamical-time background contains a disformal or otherwise non-exact transport component: even after removing known GR effects, closed-loop time transport can then retain a residual path-dependent offset. The measured "speed of light" between distant clocks is revealed as an emergent ratio of distance to accrued proper time, not a fundamental constant comparable across regions without a theory of time's flow. Locally, c remains exactly invariant; globally, dynamical time imprints tiny, path-dependent asymmetries that can be detected or bounded.

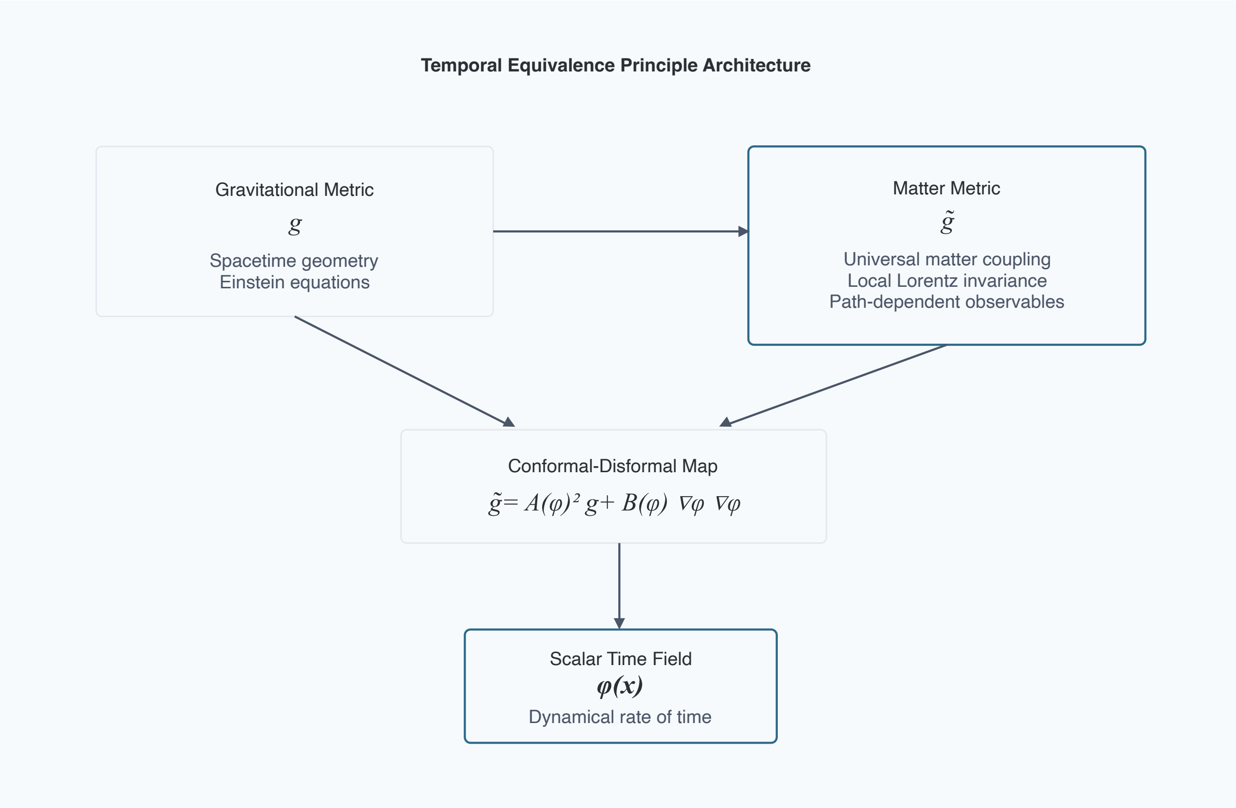

Figure 1. Temporal Equivalence Principle (TEP) architecture. Matter couples to $\tilde{g}_{\mu\nu}$ via a conformal–disformal map controlled by the scalar time field ϕ, preserving local Lorentz invariance while enabling new global invariants.

2. Axioms and the Temporal Equivalence Principle

The framework adopts four axioms:

A1. Two-metric structure on a single manifold. Gravity is described by a Lorentzian metric $g_{\mu\nu}$; matter fields, clocks, and rulers couple to a causal (matter) metric $\tilde{g}_{\mu\nu}$. The metrics are related by a disformal map

$$\tilde{g}_{\mu\nu} = A^2(\phi) g_{\mu\nu} + B(\phi)\nabla_\mu\phi\nabla_\nu\phi, \tag{1}$$

with a universal conformal factor $A(\phi) = \exp(\beta_A\phi/M_{\rm Pl})$ and a small disformal function $B(\phi)$ consistent with multi-messenger constraints today.

A2. Temporal Equivalence Principle (TEP). All non-gravitational processes evolve according to proper time $d\tau$ defined by $\tilde{g}_{\mu\nu}$: $i\hbar d|\psi\rangle/d\tau = \hat{H}|\psi\rangle$, nongravitational fields propagate on $\tilde{g}$-null cones, and ideal clocks tick $d\tau^2 = -\tilde{g}_{\mu\nu}dx^\mu dx^\nu/c^2$. In local freely falling frames for $\tilde{g}_{\mu\nu}$, physics reduces to special relativity with invariant c.

A3. Causal safety and locality. Today, $c_g = c_\gamma$ within GW170817-class bounds ($|c_g - c_\gamma|/c \lesssim \text{few} \times 10^{-15}$, with the published constraint asymmetric at this order). This is enforced by choosing $A(\phi)$ universal, such that conformal transformations preserve null cones for photons and gravitons when $B = 0$, and by constraining the observable combination $B(\phi)(\partial\phi)^2$ along late-time astrophysical propagation paths. Different experiments constrain different integrals or responses involving the single disformal function $B(\phi)$; GW170817 does not require B to vanish identically in all regimes. Hyperbolicity and energy conditions hold within the EFT domain.

A4. Screening and universality. The coupling $A(\phi)$ is universal at leading order; loop-induced composition dependence is tightly bounded. Environmental suppression of the locally observable Temporal Shear/source-charge sector reconciles local tests with cosmological dynamics. Chameleon, Vainshtein, Galileon, DBI, and symmetron mechanisms are treated as candidate microscopic completions, not as the defining ontology of TEP. Screening manifests as a continuous spatial and covariance structure of the scalar time field (Temporal Topology) governed by the temporal potential field and its gradient (Temporal Shear), suppressing fifth forces in screened regimes while leaving cosmology accessible to dynamics.

These axioms encode Einstein's local invariance as a theorem and extend it: c is exactly invariant for every tangent space of $\tilde{g}_{\mu\nu}$, but global synchronization and one-way timing depend on the dynamical field ϕ.

The scalar time field ϕ is defined on the spacetime manifold of Axiom A1 and is present at every event. The ambient cosmological value $\phi_\infty = 0$ is a boundary condition, not an absence of the field. What distinguishes dense from dilute environments is not the presence or absence of ϕ but the matter trace $T^{(\mathrm{m})}$ and the environmental state vector $\mathcal{E}$ (ambient density, compactness, gradients, boundary geometry). The term "vacuum" is retained in its standard field-theory sense — the $T^{(\mathrm{m})} = 0$ limit of the matter sector — and does not denote a region devoid of the temporal field.

Environmental screening $\mathcal{S}_\Sigma(\mathcal{E})$ suppresses the conformal gradient $\Sigma_\mu = \nabla_\mu \ln A$ — the Temporal Shear, which is the scalar fifth force — via temporal-topology pinning in dense regions. It does not suppress the disformal sector $B(\phi)$, which is governed by its own field-space envelope (Section 2.2). The two are distinct mechanisms operating on distinct sectors of the disformal map. The clock/force split ($\mathcal{S}_\Sigma \to 0$, $S_A \sim 1$) suppresses the spatial gradient while preserving the field value: $A(\phi)$ continues to vary inside screened matter, which is why clocks run slower in deeper wells. What is pinned is the gradient, not the field amplitude. Theorem 2 (Section 6) further establishes that a static conformal gradient produces no directional photon-propagation asymmetry; direction-dependent null propagation requires the disformal sector, time-dependent geometry, or another non-exact transport contribution.

Sector mapping

Sector	Physical effect	Coupling	Key bound
Conformal $A(\phi)$	Clock rates, proper time rescaling	Universal (β_A)	Cassini PPN-γ (via S_Σ source charge), redshift tests
Disformal $B(\phi)$	Null cone tilts, direction-dependent propagation	Small, environment-dependent	GW170817: $\lvert c_\gamma - c_g \rvert / c \lesssim \text{few} \times 10^{-15}$
Temporal Topology	Spatial/covariance structure of $\ln A(\phi)$	Field configuration + gradient suppression	Clock/covariance correlation length λ_T

The conformal sector governs clock rates; the disformal sector governs cone tilts. GW170817 directly bounds disformal cone splits governed by B. It does not directly test common-mode conformal clock-rate structure governed by A, although local conformal gradients/source charges remain constrained by PPN, gravitational-redshift, clock-comparison, and equivalence-principle tests.

2.1 Relation to Other Modified Gravity Frameworks

The TEP framework can be situated within the broader landscape of modified gravity and scalar-tensor theories. To clarify its unique features, a comparative analysis is provided:

Table 1: Comparison with Other Scalar-Tensor Frameworks

Theory/Framework	Key Fields	Matter Coupling	$c_g = c_\gamma$?	Key Observable Signature
TEP (This work)	$g_{\mu\nu}$, ϕ	Universal to $\tilde{g}_{\mu\nu} = A^2 g_{\mu\nu} + B \partial_\mu\phi\partial_\nu\phi$	Equal in conformal/common-mode limit; differential deviations possible through B and constrained by same-path EM–GW timing	Synchronization Holonomy H_{resid}
Horndeski	$g_{\mu\nu}$, ϕ	Minimal to $g_{\mu\nu}$	Yes, after GW170817 constraints	Modified growth, ISW
DHOST	$g_{\mu\nu}$, ϕ	Minimal to $g_{\mu\nu}$	Yes, for specific degenerate classes	Modified growth, screening
TeVeS	$g_{\mu\nu}$, A_μ, ϕ	To a combined metric	No	MOND phenomenology, lensing
SMEFT	SM fields	Lorentz-violating operators	Model-dependent	Anisotropic propagation, CPT violation

The multi-messenger constraint from GW170817 constrains the integrated EM–GW differential disformal contribution along observed late-time astrophysical paths. It does not require the disformal sector to vanish identically in all regimes. In the conformal limit, common-mode path effects cancel in EM–GW timing; residual B-sector structure remains testable through multipath delays, closed-loop holonomy, and topological or interferometric regimes. The model, with a universal conformal coupling $A(\phi)$ and a disformal term $B(\phi)$, automatically satisfies $c_g = c_\gamma$ in the conformal limit ($B = 0$). A non-zero $B(\phi)$ introduces a calculable deviation $c_\gamma \neq c_g$ constrained by future multi-messenger observations.

Conceptually, TEP differs from many scalar-tensor theories by its foundational principle: the universal coupling of matter to a single metric $\tilde{g}_{\mu\nu}$. This is philosophically closer to Bekenstein's TeVeS theory, which also introduced a separate matter metric, but the framework is more minimal, using only a scalar, and makes a distinctive operational prediction in the form of the synchronization holonomy.

2.2 Minimal covariant action

The displayed low-curvature action below represents the leading sector of the master TEP Effective Field Theory. The strong-curvature completion includes higher-order curvature operators (such as the scalar-Gauss-Bonnet coupling $\alpha_{\rm GB} f(\phi)\mathcal{G}$) which are negligible in the weak-field and cosmological regimes studied here, but become active in the strong-field regime to supply real backreaction (as detailed in TEP-BH, Paper 28). The unified action, including the strong-curvature sector, is

$$S = \int d^4x \sqrt{-g} \left[\frac{M_{\rm Pl}^2}{2} R - \frac{1}{2} K(\phi)(\nabla\phi)^2 - V(\phi) + \alpha_{\rm GB}\, f(\phi)\, \mathcal{G} \right] + S_m[\psi_i, \tilde{g}_{\mu\nu}], \tag{2}$$

with the conformal-disformal matter metric

$$\tilde{g}_{\mu\nu} = A^2(\phi)\, g_{\mu\nu} + B(\phi)\, \nabla_\mu\phi\, \nabla_\nu\phi. \tag{3}$$

In the weak-field regime ($\alpha_{\rm GB} f(\phi)\mathcal{G} \to 0$, $K \to 1$) this reduces to the minimal scalar-tensor action used throughout Papers 1–19. The strong-curvature sector is activated only in the black-hole completion (Paper 28) and does not participate in any GNSS, LLR, cosmological, or wide-binary calculation.

Canonical microscopic structure

The universal conformal coupling, the conformal–disformal matter metric architecture, and the observable Temporal-Topology response structure are fixed. TEP is not defined by a unique microscopic potential. The quartic density-dependent-mass branch provides the explicit weak-field completion used here for Solar-System and interstellar screening. The items below specify the canonical microscopic structure.

Conformal coupling. The conformal factor is fixed universally as

$$A(\phi) = \exp\left(\frac{\beta_A\, \phi}{M_{\rm Pl}} \right), \qquad \beta_A = -1.0, \tag{4}$$

so that the dimensionless DEF coupling $\alpha_0 \equiv d\ln A/d\varphi = \beta_A = -1$ is frozen, where $\varphi \equiv \phi/M_{\rm Pl}$ is the dimensionless field variable. The weak-field Solar-System safety is ensured by the screened source charge $S_\Sigma^{(\odot)}\alpha_0$: Cassini requires $|\gamma_{\rm PPN} - 1| \approx 2\alpha_0^2 (S_\Sigma^{(\odot)})^2 < 2.3 \times 10^{-5}$, fixing $S_\Sigma^{(\odot)} \lesssim 3.4 \times 10^{-3}$ in the Solar-System environment. The terrestrial amplitude factor $S_A^{(\oplus)}$ governs GNSS clock-rate and covariance observables. The Solar-System source-charge factor $S_\Sigma^{(\odot)}$ is a different projection and need not equal $S_A^{(\oplus)}$.

Sign convention for ϕ (corpus-wide). The scalar field is defined so that $\phi > 0$ **in the vicinity of a mass concentration**, with the ambient cosmological value taken as the zero point, $\phi_\infty = 0$. Combined with the frozen coupling $\beta_A = -1$, this fixes every downstream sign in the framework:

- $A(\phi) = \exp(\beta_A \varphi) < 1$ near a mass, so the conformal factor is *suppressed* in a potential well.
- Since matter clocks tick at $d\tau/dt \simeq A(\phi)$, clocks run slower in deeper wells. This reproduces the sign of the ordinary gravitational redshift and is therefore the convention consistent with general relativity in the screened limit.
- The Temporal Shear $\Sigma_\mu \equiv \nabla_\mu \ln A = \beta_A \nabla_\mu \varphi$ points *outward* from a mass (since $\beta_A < 0$ and $\nabla_\mu\varphi$ points inward).
- Consequently $\beta_A \phi < 0$ near a mass, and $\Delta \ln A < 0$ relative to the ambient environment.

The opposite choice ($\phi < 0$ near a mass, giving $A > 1$ and clocks running *faster* in wells) is inconsistent with the measured sign of gravitational redshift and is not used anywhere in this corpus. Any paper reporting a conformal-sector sign should be checked against this convention before its result is compared with another paper's. Where a manuscript quotes $|\beta_A|$ or an unsigned effective coupling, that is a magnitude and carries no sign information.

Disformal coupling. The matter metric contains a disformal coupling function $B(\phi)$. Observable disformal effects depend on the complete combination $B(\phi)\nabla_\mu\phi\nabla_\nu\phi$, rather than on $B(\phi)$ alone. Paper 28 employs the field-space envelope

$$B(\phi) = B_0\,\frac{\varphi^2}{1+\varphi^2}\,\exp\!\left(-\frac{\varphi^4}{2\,\sigma_B^4}\right), \qquad \varphi \equiv \phi/M_{\rm Pl}, \tag{5}$$

as a prescribed strong-field realization. At weak-field values ($\varphi \sim 10^{-10}$), the exponential damping factor is unity to extremely high precision and $\varphi^2/(1+\varphi^2) \simeq \varphi^2$, so $B(\phi) \simeq B_0\varphi^2$ throughout terrestrial and typical astrophysical environments. Its rapid large-$|\varphi|$ damping provides additional strong-field suppression of the disformal contribution, enforcing conformal dominance and protecting the Lorentzian matter-metric branch when scalar gradients become extreme. This field-space envelope is not identified with ordinary environmental Temporal-Topology screening, which arises primarily through the environment-dependent scalar configuration and its active gradient. The unique corpus-wide microscopic form and normalization of $B(\phi)$ therefore remain part of the action-closure problem. In the dimensionful Jakarta field convention, B_0 carries mass dimension -4 so that $B(\phi)\,\nabla_\mu\phi\,\nabla_\nu\phi$ is dimensionless; numerical normalizations employed in Paper 28's geometrized, dimensionless-field strong-field construction are therefore not imported directly into the weak-field theory. GW170817 constrains the path-integral combination $B(\phi)(\partial\phi)^2$ along observed late-time astrophysical paths; it does not require $B \equiv 0$ in every regime. The theory field ϕ remains dimensionful (mass dimension 1) throughout, consistent with the canonical kinetic term $-\frac{1}{2}(\nabla\phi)^2$ and the conformal factor $A = \exp(\beta_A\phi/M_{\rm Pl})$; φ is introduced only as a shape variable for B.

Temporal-Topology saturation sector. Environmental suppression in TEP is defined by the continuous response of the Temporal Topology rather than by a discrete density threshold or thin-shell boundary. Writing $\Theta \equiv \ln A(\phi)$ and $\Sigma_\mu \equiv \nabla_\mu\Theta$, the conformal-amplitude response S_A and the Temporal-Shear/source-charge response S_Σ are distinct observable projections of the same environment-dependent scalar configuration. The macroscopic scale

$$\rho_T \simeq 20\ \mathrm{g\,cm^{-3}} \tag{6}$$

denotes the empirically calibrated Temporal-Topology saturation/reference scale. It is not a universal microscopic density cutoff and does not define a binary screened/unscreened transition. In the weak-field, canonical $K \to 1$, $B \to 0$, quasistatic limit, a particular microscopic completion must satisfy the scalar field equation $\nabla^2\phi = V_{,\phi} + \mathcal{Q}_m$, with the matter-source convention defined consistently with the action of §2.2. Defining the conserved Einstein-frame density $\rho_* = A^3\tilde{\rho}$, the field equation reads

$$\nabla^2\phi = V_{,\phi} + \rho_*\,A_{,\phi}. \tag{7}$$

In regions where a particular completion admits an adiabatic density-dependent equilibrium, this may reduce to a local balance of the form $V_{,\phi} + \rho_*\,A_{,\phi} \simeq 0$. Such an effective minimum is one possible local realization of Temporal-Topology saturation; it is not the defining screening ontology of TEP. Chameleon, Vainshtein, Galileon, DBI, symmetron, and related mechanisms therefore remain candidate microscopic realizations rather than definitions of the framework. The quartic density-dependent-mass branch provides the explicit weak-field screening completion used here, with S_A, S_Σ, and covariance projections derived from a common action and stated boundary conditions.

Screening operators. Two projections of the solved nonlinear field configuration are needed. The field-amplitude (clock) screening S_A measures the suppression of the conformal factor excursion relative to its unscreened cosmological baseline (Paper 26, {\tt step_02_02}):

$$S_A(\mathcal{E}) \equiv \frac{\big(A(\phi(\mathbf{r}))-1\big)_{\rm local}}{\big(A(\phi)-1\big)_{\rm unscreened}}, \tag{8}$$

The source-charge (shear) screening S_Σ measures the suppression of the effective exterior scalar charge relative to the unscreened coupling:

$$S_\Sigma(\mathcal{E}) \equiv \frac{Q}{Q_0} = \frac{\alpha_{\rm eff}}{\alpha_0}, \tag{9}$$

where $\phi(\mathbf{r})$ is the solved static profile for the given source geometry, density, compactness, and boundary conditions, and Q is the effective scalar charge sourced by the body. Both are outputs of the nonlinear field equation $\Box\phi - V_{,\phi} = -\mathcal{Q}$, not phenomenological multipliers fitted separately in each domain. S_A governs clock-rate residuals and covariance; S_Σ governs PPN deviations and fifth-force bounds. The two need not be numerically identical. Strong gradient flattening suppresses S_Σ, while S_A depends separately on the local field amplitude relative to its reference environment. The mesoscopic screening law of Paper 25 ($\mathcal{S}_\Sigma^{\rm meso} = S_{\rm TEP} \times S_{\rm TF} \times S_{\rm boundary} \times S_{\rm decoherence}$) is a factorization of S_Σ at intermediate scales.

Radial ODE closure calculation. The static weak-field scalar equation $\nabla^2\phi = V_{,\phi} + \rho_* A_{,\phi}$ is solved numerically for a spherical source with the bidirectional conformal coupling $A(\phi) = \exp(-\phi/M_{\rm Pl})$, $\beta_A = -1$, using `scipy.integrate.solve_bvp` with core regularity ($\phi'(0) = 0$) and cosmological relaxation ($\phi(r_{\rm max}) \to 0$) boundary conditions (`scripts/steps/step_01_radial_ode.py`, output in `results/step_01_radial_ode.json`). The key dimensionless parameter is the unscreened field amplitude $\psi_{\rm uns} = M/(4\pi M_{\rm Pl}^2 R)$, which controls the strength of the conformal nonlinearity: $\psi_{\rm uns}(\odot) \simeq 4.2 \times 10^{-6}$, $\psi_{\rm uns}({\rm NS}) \simeq 0.41$, $\psi_{\rm uns}({\rm BH}) \simeq 1.0$. Three candidate potentials are tested against the Cassini bound $|\gamma_{\rm PPN} - 1| < 2.3 \times 10^{-5}$ (requiring $S_\Sigma^{(\odot)} \lesssim 3.4 \times 10^{-3}$ at 1 AU):

(i) $V = 0$ (pure bidirectional conformal screening). The nonlinear source $-(\rho_*/M_{\rm Pl})\exp(-\phi/M_{\rm Pl})$ provides gradient flattening in overdensities ($\phi > 0$, $\exp(-\phi/M_{\rm Pl}) < 1$, source weakened) and enhancement in underdensities ($\phi < 0$, $\exp(-\phi/M_{\rm Pl}) > 1$). The screening correction is $O(\psi_{\rm uns}) \sim 4 \times 10^{-6}$ for the Sun — three orders of magnitude below the Cassini requirement. The conformal nonlinearity alone is too weak for Solar-System screening.

(ii) $V = \lambda\phi^4/4$ (quartic, density-dependent mass). The cubic derivative $V_{,\phi} = \lambda\phi^3$ yields an effective mass $m_{\rm eff}^2 = 3\lambda\phi_{\rm min}^2 \propto \rho^{2/3}$, which is large in dense solar material and tiny in the interstellar medium. The dimensionless coupling relates to the physical parameter via $\mu_0 = \lambda[M_\odot/(4\pi M_{\rm Pl})]^2 \approx 1.33 \times 10^{75}\,\lambda$, so $\mu_0 = 10^5$ corresponds to dimensionless physical self-coupling $\lambda \approx 7.52 \times 10^{-71}$ (with canonical mass dimension $[\phi] = 1$ in 4D). An extended scan with continuation from lower coupling strengths finds that the Cassini threshold is crossed at $\mu_0 \gtrsim 3 \times 10^4$: $S_\Sigma(1\,{\rm AU}) = 2.65 \times 10^{-3}$ at $\mu_0 = 3 \times 10^4$, 1.46×10^{-3} at $\mu_0 = 10^5$, and 4.68×10^{-4} at $\mu_0 = 10^6$. The solar-interior Compton length is $\lambda_{c,\odot} \approx 2.7 \times 10^{-4}$ AU ($\approx 0.059\,R_\odot$), enforcing continuous gradient screening, while the ISM Compton length is $\lambda_{c,{\rm ISM}} \approx 1.33$ pc ($\approx 2.7 \times 10^5$ AU), preserving the ambient environmental field structure across wide-binary scales. The quartic behaves as a density-dependent-mass completion: the same parameter set screens the solar perturbation at 1 AU while remaining ultralight in the interstellar medium.

(iii) $V = \frac{1}{2}m^2\phi^2$ (quadratic/Yukawa). The linear derivative $V_{,\phi} = m^2\phi$ provides efficient screening for small fields, and the exterior solution exhibits Yukawa decay $\phi \propto e^{-\sqrt{\mu_0}\,x}/x$. Cassini is satisfied for effective mass parameter $\mu_0 \geq 0.01$, with $S_\Sigma(1\,{\rm AU}) \leq 10^{-8}$ and $|\gamma - 1| \leq 10^{-16}$. However, no single μ_0 simultaneously satisfies Cassini and leaves wide binaries (at ~ 2646 AU) unscreened: the Cassini requirement $\mu_0 \gtrsim 0.01$ and the wide-binary requirement $\mu_0 \lesssim 10^{-12}$ are separated by ten orders of magnitude. This gap is intrinsic to any single-mass Yukawa potential.

A three-zone density profile (solar interior, interplanetary medium at $\rho_{\rm ip}/\rho_\odot \sim 10^{-25}$, interstellar medium at $\rho_{\rm ism}/\rho_\odot \sim 10^{-27}$) confirms that the conformal coupling provides a density-dependent effective mass $m_{\rm eff}^2 = m^2 + (\rho/M_{\rm Pl}^2)\exp(-\phi/M_{\rm Pl})$, but the density-dependent contribution is negligible at both 1 AU and 2646 AU because the ambient densities are 10^{25}–10^{27} times below the solar density. Wide binaries become unscreened only at $\rho_{\rm ism}/\rho_\odot \sim 10^{-15}$, twelve orders of magnitude above the physical interstellar density.

The radial ODE closure status is therefore: Cassini is satisfied by $V = \frac{1}{2}m^2\phi^2$ with $\mu_0 \geq 0.01$ and by $V = \lambda\phi^4/4$ with $\mu_0 \gtrsim 3 \times 10^4$. The single-mass Yukawa ten-order gap between the Cassini and wide-binary requirements is resolved by the density-dependent-mass quartic, whose $m_{\rm eff} \propto \rho^{1/3}$ is large in dense solar material (Compton length $\sim 2.7 \times 10^{-4}$ AU) and tiny in the interstellar medium (Compton length ~ 1.33 pc). The wide-binary signal reflects the recovery of the stellar Temporal Shear against the Galactic environmental floor, not an isolated solar field extending to 2646 AU: the ambient Galactic field dominates the local stellar field perturbation by $\sim 10^7$ at wide-binary separations across the full stellar population ($M \approx 0.1$–$8\,M_\odot$), setting the local screening floor and enabling the binary's internal Temporal Shear to recover. The wide-binary screening radius is quantitatively derived: the cross-scale acceleration condition $g_N(R_s) \approx 2g_{\rm TEP}$ predicts $R_s^{\rm pred} \approx 2709$ AU for $M = 1.24\,M_\odot$ (matching the headline fit 2646 ± 182 AU within 3% and lying squarely within the ~ 2.6–7.1 kAU range spanned by stratified environmental subsets), and the mass-convolved model $R_s(M) \propto M^{1/3}$ yields $R_s = 2612$ AU for a typical $1.25\,M_\odot$ primary: the fixed-$g_{\rm TEP}$ acceleration threshold yields the fiducial $R_s \propto M^{1/2}$ cross-scale estimate, while the population-level screening relation after environmental density convolution follows the calibrated $R_s \propto M^{1/3}$ law. Across all stellar types, the continuous gradient suppression factor scales as $M^{-2/3}$, so lower-mass stars experience stronger relative suppression; the residual source charge S_Σ increases with mass and retains a compactness dependence (whereas the population-level velocity-excess amplitude incorporates the orbital Keplerian baseline, naturally yielding a larger fractional boost in lower-mass binaries), yet every stellar archetype remains below the Cassini bound at 1 AU while recovering the Galactic Temporal Shear at wide-binary scales. The bidirectional conformal mechanism provides the framework (symmetric A around unity, conformal excursions averaging along lines of sight, non-exact covariance $\mathcal{C}_T$ surviving averaging); the density-dependent-mass quartic is a candidate completion, not a definition of the framework. This is consistent with the framework's design: $V(\phi)$ is not uniquely fixed, and chameleon, Vainshtein, Galileon, DBI, and symmetron mechanisms remain candidate microscopic completions rather than definitions.

Cassini constraint interpretation. The Cassini Shapiro-delay measurement is a round-trip radio ranging experiment performed during solar conjunction, where signals passed through the Sun's deep gravitational potential. Two features of this configuration are relevant for TEP. First, the geometric Shapiro delay, governed by the gravitational metric $g_{\mu\nu}$ and the PPN parameter γ, is a path integral of the metric perturbation; the outbound and inbound integrals add (doubling the delay), so this effect does not cancel. The conformal clock variation, governed by $A(\phi)$ through the matter metric $\tilde{g}_{\mu\nu} = A^2 g_{\mu\nu}$, enters the signal as a gradient integral $\int \nabla(\ln A) \cdot d\mathbf{l}$; the outbound integral has the opposite sign to the inbound integral (the path is traversed in the opposite direction), so the conformal clock contribution cancels exactly in the round-trip. The conformal factor A^2 also preserves null cones ($0 = A^2(-dt^2 + dl^2) \Rightarrow dt = dl$), so $A(\phi)$ does not affect light propagation directly. Cassini therefore constrains the source-charge/shear sector S_Σ (the scalar field's contribution to $g_{\mu\nu}$ through $T^{(\phi)}_{\mu\nu}$), not the clock/amplitude sector S_A (the conformal factor $A(\phi)$ itself). Second, and more importantly, the Cassini signal path samples the Sun's deep potential well, which in TEP corresponds to the screened regime: the TEP scalar equation $\nabla^2\phi = V_{,\phi} + \rho_* A_{,\phi}$ admits a density-dependent field minimum at $V_{,\phi} + \rho_* A_{,\phi} = 0$, at which the gradient vanishes ($S_\Sigma \to 0$) and $\gamma_{\mathrm{PPN}} \to 1$. The Cassini measurement therefore probes the screened regime, where the effective scalar charge $S_\Sigma^{(\odot)}$ is suppressed and γ_{PPN} is close to unity. The bound $S_\Sigma^{(\odot)} \lesssim 3.4 \times 10^{-3}$ applies to the solar-vicinity environment along the signal path, not to the dilute interstellar medium where the field gradient recovers and wide-binary dynamics originate. Suitable potential completions, including the quartic branch demonstrated here and chameleon- or symmetron-like realizations, admit density-dependent equilibria; derivative-screened completions such as Vainshtein/Galileon or DBI realize environmental suppression through different nonlinear structures. The Cassini constraint is therefore environment-specific: it bounds the screened solar source-charge projection $S_\Sigma^{(\odot)}$, not the recovered interstellar response relevant to wide binaries.

Wide-binary and cross-scale consistency. The wide-binary velocity excess (Paper 13, $\alpha_{\mathrm{sat}} = 0.366 \pm 0.012$, $R_s = 2646 \pm 182$ AU) is a force-sector observable: the acceleration $\mathbf{a}_{\mathrm{eff}} = -\nabla\Phi_N - c^2 \mathcal{S}_\Sigma(\mathcal{E})\, \nabla \ln A$ is governed by the Temporal Shear gradient $\nabla \ln A$, which is the S_Σ projection. The conformal amplitude $A(\phi)$ does not separately enter the velocity ratio, because the conformal factor cancels in $\tilde{v} = d\tilde{l}/d\tilde{\tau} = (A\, dl)/(A\, d\tau) = v$. The ten-order-of-magnitude gap between the Cassini and wide-binary single-mass Yukawa requirements is therefore environmental, not sectoral: S_Σ is suppressed in the high-density solar vicinity (Cassini, screened) and recovers in the dilute interstellar medium (wide binaries, unscreened). The density-dependent minimum of the TEP field equation $\nabla^2\phi = V_{,\phi} + \rho_* A_{,\phi}$ provides the environmental transition; the quartic completion $V = \lambda\phi^4/4$ realises this with $m_{\mathrm{eff}} \propto \rho^{1/3}$, screening at 1 AU while preserving a ~ 1 pc Compton length in the ISM. The cross-scale architecture is the strongest evidence: the GNSS covariance length $\lambda_T \approx 4200$ km (Paper 1) calibrates the Temporal Topology saturation scale $\rho_T \approx 20$ g/cm^3 (Paper 6) through $R_T(M_\oplus) = L_c$, fixing the terrestrial scale. Independently, the SPARC-derived characteristic acceleration $g_{\mathrm{TEP}} \approx 5 \times 10^{-10}$ m/s^2 (Paper 10)—rooted in the cosmological horizon acceleration scale $g_t \sim cH_0/2 \approx 3.4 \times 10^{-10}$ m/s^2 and matching the ambient Galactic shear $a_{\mathrm{amb}} \approx 3.9 \times 10^{-10}$ m/s^2 at the solar circle—predicts the wide-binary screening radius $R_s^{\mathrm{pred}} = \sqrt{GM/(2g_{\mathrm{TEP}})} \approx 2709$ AU with no wide-binary input (matching the headline fit 2646 ± 182 AU to within 3% with the Galactic external field floor $\eta = 2$, and lying squarely within the range spanned by stratified environmental subsets, ~ 2.6–7.1 kAU); and the Earth-flyby suppression $S_\oplus \approx 0.35$ (Paper 15) is consistent with $(R_\oplus - R_T)/R_\oplus$. These scales span eight orders of magnitude in distance and are anchored by distinct observational inputs, not by the Cassini bound.

Recovery operator — defining constraints. Locally the time field recovers Temporal Shear (a real force) only in low-acceleration, two-source configurations, and saturates everywhere else. The recovery operator is fixed by six constraints: F1 — excludes the inverse-power thin-shell branch: with $\beta_A = -1$, the inverse-power potential has no admissible minimum and predicts the wrong environmental direction; F2 — not a pure gradient cap $P(X)$ (a gradient-cap scale $g_{\mathrm{cap}} \sim g_{\mathrm{TEP}}$ would leave an unsuppressed Solar-System acceleration floor $\approx 2\beta^2 g_{\mathrm{cap}} \approx 10^{-9}$ m s^{-2}, $10^5\times$ the Saturn bound); F3 — $K > 3\Omega_m$ (stability bound from §2.2); F4 — per-system recovery steepness $k \geq 4$ in separation (theorem + wide-binary data); F5 — transition radius larger in denser environments, amplitude rises with mass ratio q, transition radius grows as $R_s \propto M^{1/3}$ while amplitude falls with primary mass (weaker self-screening in lower-mass systems revealing larger unsuppressed response; measured, Paper 13); F6 — environmental coupling normalisation differs by ≈ 4–6% between host disks and anchors (measured, §7.4). The canonical exponential is a population curve; each system recovers steeply, $f_i(s) = [1 + (R_i/s)^k]^{-1}$, with transition radii R_i spread by the environmental state. The operator is fixed by what it must do, not by an assumed potential.

Variation with respect to the Einstein-frame metric, ϕ, and matter fields gives the Einstein-frame field equations, scalar equation of motion, and matter-frame conservation law.

2.3 Field equations and conservation laws

The field equations below are the low-curvature $K \to 1$, $\alpha_{\mathrm{GB}} f(\phi)\mathcal{G} \to 0$ equations relevant to the sectors considered in this paper (GNSS, LLR, cosmological background, wide binaries). The strong-curvature sector is invoked only in the black-hole completion (Paper 28). Varying the action with respect to the Einstein-frame metric, ϕ, and the matter fields yields three sets of equations.

Einstein-frame field equations

$$G_{\mu\nu} = \frac{1}{M_{\rm Pl}^2}\left[T^{(\phi)}_{\mu\nu} + T^{(m)}_{\mu\nu}\right], \tag{10}$$

with the scalar stress-energy

$$T^{(\phi)}_{\mu\nu} = \nabla_\mu\phi\nabla_\nu\phi - g_{\mu\nu}\left[\frac{1}{2}(\nabla\phi)^2 + V(\phi)\right]. \tag{11}$$

The Einstein-frame matter stress-energy $T^{(m)}_{\mu\nu}$ is obtained from $S_m[\tilde{g}]$ by functional differentiation with respect to the inverse Einstein-frame metric $g^{\mu\nu}$:

$$T^{(m)}_{\mu\nu} = -\frac{2}{\sqrt{-g}}\frac{\delta S_m}{\delta g^{\mu\nu}} = \frac{\sqrt{-\tilde{g}}}{\sqrt{-g}}\,\tilde{T}^{(m)}_{\alpha\beta}\,\frac{\partial\tilde{g}^{\alpha\beta}}{\partial g^{\mu\nu}}, \tag{12}$$

where $\tilde{T}^{(m)}_{\alpha\beta} = -\frac{2}{\sqrt{-\tilde{g}}}\frac{\delta S_m}{\delta\tilde{g}^{\alpha\beta}}$ is the matter-frame stress-energy. For the disformal inverse

$$\tilde{g}^{\mu\nu} = A^{-2}\left[g^{\mu\nu} - \frac{(B/A^2)\,\partial^\mu\phi\,\partial^\nu\phi}{1 + (B/A^2)(\partial\phi)^2}\right], \tag{13}$$

the Jacobian $\partial\tilde{g}^{\alpha\beta}/\partial g^{\mu\nu}$ yields, at leading order in small B,

$$T^{(m)}_{\mu\nu} = A^2(\phi)\,\tilde{T}^{(m)}_{\mu\nu} + O(B). \tag{14}$$

Thus the Einstein-frame equations reduce to a scalar-tensor theory with conformally-coupled matter at leading order; disformal corrections enter at $O(B)$ and are suppressed by the same multi-messenger bounds that constrain the light-cone tilt.

Scalar equation of motion

For the scalar equation it is useful to define the matter-frame stress tensor by

$$\tilde{T}^{\mu\nu} \equiv \frac{2}{\sqrt{-\tilde{g}}}\frac{\delta S_m}{\delta\tilde{g}_{\mu\nu}}. \tag{15}$$

This is equivalent to the covariant definition

$$\tilde{T}_{\mu\nu} = -\frac{2}{\sqrt{-\tilde{g}}}\frac{\delta S_m}{\delta\tilde{g}^{\mu\nu}}, \tag{16}$$

with indices raised and lowered using $\tilde{g}_{\mu\nu}$.

The density-weighted tensor is also defined as

$$\mathcal{T}^{\mu\nu} \equiv \frac{\sqrt{-\tilde{g}}}{\sqrt{-g}} \tilde{T}^{\mu\nu}. \tag{17}$$

Varying the matter metric with respect to ϕ gives

$$\delta_\phi \tilde{g}_{\mu\nu} = 2AA_{,\phi} g_{\mu\nu} \delta\phi + B_{,\phi} \nabla_\mu \phi \nabla_\nu \phi \, \delta\phi + B \left(\nabla_\mu \delta\phi \, \nabla_\nu \phi + \nabla_\mu \phi \, \nabla_\nu \delta\phi \right). \tag{18}$$

After integrating the derivative terms by parts, the scalar equation can be written as

$$\Box\phi - V_{,\phi} = -\mathcal{Q}, \tag{19}$$

where

$$\mathcal{Q} = AA_{,\phi} g_{\mu\nu} \mathcal{T}^{\mu\nu} + \frac{1}{2} B_{,\phi} \mathcal{T}^{\mu\nu} \nabla_\mu \phi \nabla_\nu \phi - \nabla_\mu \left(B \mathcal{T}^{\mu\nu} \nabla_\nu \phi \right). \tag{20}$$

Equivalently,

$$\Box\phi = V_{,\phi} - AA_{,\phi} g_{\mu\nu} \mathcal{T}^{\mu\nu} - \frac{1}{2} B_{,\phi} \mathcal{T}^{\mu\nu} \nabla_\mu \phi \nabla_\nu \phi + \nabla_\mu \left(B \mathcal{T}^{\mu\nu} \nabla_\nu \phi \right). \tag{21}$$

In the conformal limit $B \to 0$, this reduces to the standard conformally coupled scalar-tensor source equation,

$$\Box\phi - V_{,\phi} = -AA_{,\phi} g_{\mu\nu} \mathcal{T}^{\mu\nu}. \tag{22}$$

Equivalently, in terms of the effective scalar coupling

$$\alpha(\phi) \equiv \frac{d \ln A}{d\phi}, \tag{23}$$

the conformal source is proportional to the matter trace. Nonrelativistic matter sources the scalar through $T \simeq -\rho$, while radiation with $T \simeq 0$ weakly sources the conformal sector, as used in the cosmological discussion.

Matter-frame conservation law

$$\tilde{\nabla}_\mu \tilde{T}^{\mu\nu}_{(m)} = 0, \tag{24}$$

which follows from diffeomorphism invariance of $S_m[\tilde{g}]$ and implies that non-gravitational test particles and light follow geodesics of the matter metric $\tilde{g}_{\mu\nu}$. In the Einstein frame, matter and the scalar exchange energy-momentum. Diffeomorphism invariance gives

$$\nabla_\mu T^{\mu\nu}_{(m)} = \mathcal{Q} \nabla^\nu \phi, \tag{25}$$

while the scalar stress tensor satisfies

$$\nabla_\mu T^{\mu\nu}_{(\phi)} = -\mathcal{Q}\nabla^\nu \phi. \tag{26}$$

Therefore the total Einstein-frame stress tensor is conserved:

$$\nabla_\mu \left(T^{\mu\nu}_{(m)} + T^{\mu\nu}_{(\phi)}\right) = 0. \tag{27}$$

The matter-frame conservation law remains

$$\tilde{\nabla}_\mu \tilde{T}^{\mu\nu}_{(m)} = 0, \tag{28}$$

because matter is minimally coupled to $\tilde{g}_{\mu\nu}$.

These equations define the EFT structure used throughout the paper. The scalar source $\mathcal{Q}$ displays the leading conformal-disformal matter coupling explicitly.

3. Operational Foundations: Measurement, Simultaneity, and One-Way Light

3.1 What is actually measured

No measurement of c uses null proper time along the photon's worldline; that would be $c = dx/d\tau$ with $d\tau = 0$. Instead, a distance is compared with an elapsed proper time on an observer's clock. For two spatially separated clocks A and B with worldlines γ_A, γ_B and a light path λ from A to B, the measured one-way time t_{AB} is the difference in B's proper time between emission and reception, after a synchronization convention has assigned simultaneity between A and B. Two-way measurements are convention-independent; one-way measurements are not, unless an invariant observable is provided.

3.2 The synchronization problem in a dynamical-time background

Einstein synchronization assumes (i) reciprocity of propagation and (ii) homogeneity of time standards along the path. If the rate $d\tau/dt$ varies spatially or directionally, synchronization by light exchange over extended loops becomes path-dependent. The proper formalism invokes the congruence u_μ of observers (clocks) and the null geodesics k^μ of $\tilde{g}_{\mu\nu}$. Define simultaneity as orthogonality to u_μ (where Frobenius integrability allows it), and define time transport by mapping a proper-time interval at A to B using $\tilde{g}$-null signals. In GR, the non-closure of such transports arises from rotation of the congruence (vorticity) and spacetime curvature (Sagnac/Shapiro); both can be modeled and removed. In a dynamical-time geometry with disformal couplings, there is an additional, tiny non-exact contribution to time transport that cannot be removed by coordinate choices: a synchronization holonomy.

3.3 A convention-independent observable: synchronization holonomy

The operational observable is not a raw one-way speed and not the integral of a scalar proper-time differential. It is the residual non-closure of synchronization transport around a closed loop after subtracting the GR prediction.

Let $\tilde{\sigma}$ denote the matter-frame synchronization transport one-form induced by $\tilde{g}_{\mu\nu}$ and the chosen clock congruence, and let σ_{GR} denote the corresponding GR one-form including Sagnac, gravitomagnetic / Lense–Thirring, Shapiro delay, gravitational redshift, station motion, clock-scale realization, and reference-frame corrections. The residual holonomy is:

$$H_{\mathrm{resid}}(C) \equiv \oint_C (\tilde{\sigma} - \sigma_{\mathrm{GR}}) = \iint_\Sigma (d\tilde{\sigma} - d\sigma_{\mathrm{GR}}), \qquad C = \partial\Sigma. \tag{29}$$

Equivalently, defining $\tilde{F} = d\tilde{\sigma}$ and $F_{\mathrm{GR}} = d\sigma_{\mathrm{GR}}$:

$$H_{\mathrm{resid}}(C) = \iint_{\Sigma} (\tilde{F} - F_{\mathrm{GR}}). \tag{30}$$

This quantity is invariant under admissible synchronization re-gaugings because the matter-frame connection $\tilde{\sigma}$ and the corresponding GR reference connection σ_{GR} shift by the same exact one-form, leaving the residual connection $\Delta\sigma = \tilde{\sigma} - \sigma_{\mathrm{GR}}$ unchanged. Equivalently, any representative shift by an exact form integrates to zero around a closed loop.

Conformal exactness and vanishing loop holonomy

In the conformal-only subclass ($B = 0$), the scalar contribution to local clock-rate transport is generated by the exact one-form $\omega^{(A)} = d \ln A$. For any closed loop C in a simply connected region where $A(\phi)$ is smooth and single-valued:

$$\oint_C \omega^{(A)} = \oint_C d \ln A = 0. \tag{31}$$

Thus a conformal-only scalar may affect local rates and open-path redshift comparisons, but it cannot by itself generate a closed-loop residual synchronization holonomy. A leading-order nonzero H_{resid} requires residual synchronization curvature $d(\tilde{\sigma} - \sigma_{\mathrm{GR}}) \neq 0$, which in this framework arises from the disformal sector, non-metricity, or other explicitly non-exact transport structure.

This reframes "variable c" claims: the invariant diagnostic is not a raw one-way c, but H_{resid}. A nonzero H_{resid} means simultaneity is not integrable beyond GR; this is what dynamic time does to measurement.

Figure 2. Synchronization holonomy on a spacelike slice in the matter frame. The residual invariant H_{resid} subtracts all GR corrections (Sagnac, gravitomagnetic / Lense–Thirring, Shapiro delay, gravitational redshift, station motion, clock-scale realization, and reference-frame corrections), isolating dynamical-time effects.

4. Disformal Invertibility, Causality, and Hyperbolicity

Invertibility and signature

The inverse of $\tilde{g}_{\mu\nu}$ exists for $A > 0$ and $1 + (B/A^2)(\partial\phi)^2 \neq 0$:

$$\tilde{g}^{\mu\nu} = A^{-2} \left[g^{\mu\nu} - \frac{(B/A^2)\partial^\mu\phi\partial^\nu\phi}{1 + (B/A^2)(\partial\phi)^2} \right]. \tag{32}$$

For Lorentzian signature, require $A > 0$ and $B(\partial\phi)^2 > -A^2$. B is assumed small and gradients bounded in all regimes of interest.

Causality

The matter cone is inside or equal to the gravitational cone when $B \geq 0$ and gradients are modest; no closed causal curves arise for small B. When the observable disformal deformation $\frac{B(\phi)}{A^2(\phi)}(\partial\phi)^2$ is negligible along the relevant late-time propagation paths, gravitational and matter null cones coincide to the required observational accuracy. Laboratory resonator tests independently constrain orientation-dependent components of the same local disformal deformation in the terrestrial environment, while multi-messenger observations strongly constrain its integrated realization along astrophysical propagation paths. These constraints bound the complete disformal deformation on the realized scalar background rather than requiring $B(\phi)$ itself to vanish identically. With B small, any phase differences in propagation are minute and bounded by multi-messenger results.

Hyperbolicity

The canonical scalar equation has a hyperbolic principal operator on a Lorentzian background; $V'' > 0$ supplies positive-mass stability near an equilibrium. In the small-disformal EFT used here the theory is treated perturbatively about that background. Strong hyperbolicity of a complete nonlinear realization requires analysis of the coupled principal symbol and is not claimed in this paper. Multi-messenger observations strongly constrain the relevant late-time disformal combinations along astrophysical paths, while the realized background solution must independently satisfy the signature condition in other environments. Within the small-B, canonical-scalar EFT regime considered here, no ghost or gradient instability is introduced at leading order. The EFT is valid below the disformal scale M, with higher-dimensional operators suppressed. The specific phenomenological window for the cutoff scale M is bounded from below by the requirement that the EFT remains strictly valid across terrestrial and solar-system density gradients, and from above by the requirement that $B(\phi)$ generates a detectable macroscopic holonomy without violating the $|c_\gamma - c_g|/c$ multi-messenger constraints.

5. Local Lorentz Invariance, Proper Time, and the Emergence of c

Proper time

Clocks measure $d\tau^2 = -\tilde{g}_{\mu\nu} dx^\mu dx^\nu / c^2$. In a local lab with small velocities and $\partial_0 \phi \ll |\nabla \phi|$, $-\tilde{g}_{00} \approx A(\phi)^2(-g_{00}) - B(\partial_0 \phi)^2$, so

$$\frac{d\tilde{\tau}}{d\tau_g} = A(\phi), \tag{33}$$

up to $O(B)$ corrections. This "dynamical time law" rescales all frequency standards locally.

Local c

All small labs measure an invariant c; the conformal factor rescales both clocks and rulers uniformly, preserving null cones. Thus the empirical fact "c is constant" remains a theorem of the theory at the local level.

Global measures

Global "speeds" involve synchronized endpoints. Because the matter metric depends on the dynamical temporal field, global synchronization can acquire non-integrability when the resulting transport contains a disformal or otherwise non-exact component. That non-integrability—not a local violation of Lorentz invariance—is the source of observable departures.

6. Synchronization in a Dynamical Time: One-Way Light and Holonomy

Operational definitions

Two-way light speed is synchronization-independent and has established c's local invariance. One-way measures require synchronized clocks at A and B; Einstein synchronization assumes time-orthogonal slices and propagation symmetry. In a dynamical ϕ background, slow clock transport and one-way synchronization are path and history dependent.

Key theorems

Theorem 1 (Conformal null-cone invariance)

For $\tilde{g}_{\mu\nu} = A(\phi)^2 g_{\mu\nu}$, null vectors of $g_{\mu\nu}$ are null for $\tilde{g}_{\mu\nu}$. Maxwell's action is conformally invariant in 4D, so photon trajectories are null with respect to both metrics. Gravitational and electromagnetic waves share null cones when $B = 0$ at late times.

Theorem 2 (Exact direct conformal propagation null)

In the purely conformal limit $B = 0$, the multiplicative conformal factor $A^2(\phi)$ preserves the null cone exactly. A static conformal rescaling therefore produces no direct direction-odd same-path photon-propagation delay:

$$\Delta t^{(A)}_{\rm prop} = 0. \tag{34}$$

The conformal clock connection is exact, $\omega^{(A)} = d \ln A$, and hence $\oint_C d \ln A = 0$ in a smooth simply connected region. Observable conformal effects remain possible through clock-rate differences, accumulated proper-time histories, and open-path redshift comparisons. Scalar-induced backreaction on $g_{\mu\nu}$, time-dependent geometry, the disformal sector, or another non-exact transport structure are separate channels and are not excluded by this theorem.

Proof sketch. *For $\tilde{g}_{\mu\nu} = A^2(\phi)\, g_{\mu\nu}$ with $B = 0$, a photon null condition $\tilde{g}_{\mu\nu} k^\mu k^\nu = 0$ reduces to $g_{\mu\nu} k^\mu k^\nu = 0$ because $A > 0$. The conformal factor therefore cancels exactly from the null propagation condition and cannot act as a direction-dependent refractive index; see Appendix A2 for the full derivation.*

Synchronization one-form and holonomy

Decompose $\tilde{g}_{\mu\nu}$ in 3+1 form:

$$\tilde{g}_{\mu\nu} dx^\mu dx^\nu = -\tilde{N}^2 dt^2 + \tilde{h}_{ij}(dx^i + \tilde{N}^i dt)(dx^j + \tilde{N}^j dt). \tag{35}$$

Define the coordinate synchronization connection by the threading representative

$$\tilde{\sigma}_i = \frac{\tilde{g}_{0i}}{\tilde{g}_{00}}, \tag{36}$$

up to the overall sign convention adopted for simultaneity transport. In ADM variables, for small shift,

$$\tilde{\sigma}_i \simeq -\frac{\tilde{N}_i}{\tilde{N}^2}. \tag{37}$$

A proper-time-normalized representative differs by a factor of the lapse; all closed-loop observables below use the same representative for both $\tilde{\sigma}$ and $\sigma_{\rm GR}$, so the GR-subtracted residual is unaffected by this normalization choice. For a closed spatial loop C, the raw loop integral is

$$H = \oint_C \tilde{\sigma}, \tag{38}$$

but the physical TEP observable is the GR-subtracted residual

$$H_{\rm resid}(C) = \oint_C (\tilde{\sigma} - \sigma_{\rm GR}) = \iint_\Sigma (d\tilde{\sigma} - d\sigma_{\rm GR}), \qquad C = \partial\Sigma. \tag{39}$$

In GR with stationary spacetimes, the raw holonomy reproduces the Sagnac/gravito-magnetic effect; these known contributions are subtracted using geodesy and ephemerides. The residual holonomy beyond GR is therefore

$$H_{\mathrm{resid}}(C) = \iint_{\Sigma} (d\tilde{\sigma} - d\sigma_{\mathrm{GR}}), \qquad C = \partial\Sigma, \tag{40}$$

where σ_{GR} includes the standard Sagnac, gravitomagnetic/Lense--Thirring, Shapiro, gravitational-redshift, station-motion, clock-scale, and reference-frame contributions. This residual vanishes in SR/GR with $B = 0$ and stationary A; it is generically nonzero with disformal corrections ($B \neq 0$) and/or temporal variation of A combined with motion through $\nabla\phi$. Configurations in which C does not bound a smooth surface — non-simply-connected transport, or a connection that is locally closed but not globally exact — are not described by this Stokes expression and are treated as a separate topological case in Appendix A3.

Gauge and protocol invariance

$\tilde{\sigma}$ and σ_{GR} are synchronization-connection representatives for the same physical clock network and the same loop, evaluated in the matter-frame model and the corresponding GR reference model respectively. A synchronization re-gauging $t \to t + \chi(x^i)$ shifts both representatives by the same exact one-form. Therefore the GR-subtracted connection

$$\Delta\sigma = \tilde{\sigma} - \sigma_{\mathrm{GR}} \tag{41}$$

and its closed-loop integral

$$H_{\mathrm{resid}}(C) = \oint_C \Delta\sigma \tag{42}$$

are invariant under admissible synchronization changes. This addresses the critique that holonomy is conventional: the observable is the residual loop class of $\Delta\sigma$, not the exact part of any raw one-way synchronization convention.

Disformal corrections to $\tilde{\sigma}$

For small B and modest $\partial\phi$,

$$\tilde{N} \approx AN\left[1 - \frac{B}{2A^2N^2}(n\cdot\partial\phi)^2\right], \quad \tilde{N}_i \approx A\left[N_i + \frac{B}{A^2}(\partial_i\phi)(n\cdot\partial\phi)\right], \tag{43}$$

with n^μ the unit normal to slices. Then $\delta\tilde{\sigma}$ denotes the leading disformal correction to the chosen synchronization representative. Its covariant clock-congruence form is derived in Appendix A3; in a hypersurface-orthogonal $3+1$ slicing it reduces, up to lapse/shift convention and overall sign, to the expression proportional to

$$-\frac{B}{A^2N}(\partial_i\phi)(n\cdot\partial\phi)\,dx^i. \tag{44}$$

At leading order beyond the GR-subtracted reference model,

$$d(\Delta\sigma) = d(\tilde{\sigma} - \sigma_{\mathrm{GR}}) \supset d(\delta\tilde{\sigma}), \tag{45}$$

where the Δ indicates the residual beyond GR. Time dependence of ϕ and motion through $\nabla\phi$ generate non-vanishing curl.

7. Screening, PPN, Equivalence Principle, and Disformal Bounds

Screening

Screening in TEP is described as suppression of the locally observable Temporal Shear/source-charge sector, not as a commitment to a specific chameleon, Vainshtein, Galileon, DBI, or symmetron microphysics. Those mechanisms may be studied as candidate completions. In the effective theory used here, screening is expressed through the conformal factor $\ln A(\phi)$, its gradient Σ_μ, and its covariance C_A. Source structure, environmental state, and boundary conditions suppress the locally active shear sector in screened regimes.

The saturation scale ρ_T denotes the Temporal Topology saturation scale. It is not a local on/off condition of the form $\rho > \rho_T \Rightarrow$ GR and $\rho < \rho_T \Rightarrow$ active. Recovery of GR in local tests is controlled by suppression of the observable shear/source-charge sector, $\Sigma_\mu^{\text{obs}} = \mathcal{S}_\Sigma(\mathcal{E})\Sigma_\mu$ with $\mathcal{S}_\Sigma \to 0$ in screened regimes, where $\mathcal{E}$ includes source structure, environment, boundary conditions, and density.

Screening is not a single density switch. It is an environmental suppression operator $\mathcal{S}_\Sigma(\mathcal{E})$ whose observable projection depends on scale. The environmental state $\mathcal{E}$ includes: ambient density ρ, gravitational compactness Φ/c^2, density gradients $\nabla\rho$, potential gradients $\nabla\Phi$, proximity to field sources, coherence volume, boundary geometry, and asymptotic horizon proximity. Each domain uses a different projection of $\mathcal{E}$:

- **GNSS/clock covariance:** spatial covariance / Earth-scale saturation projection of $\mathcal{S}_\Sigma(\mathcal{E})$.
- **UCD/galaxy scales:** mass-radius-density saturation projection through the geometric scale $R_T(M)$.
- **NIST/laboratory G:** lab-scale geophysical column projection of $\mathcal{S}_\Sigma(\mathcal{E})$.
- **MSP pulsars:** cluster-potential response with stellar/environmental transfer.
- **Cepheids:** galactic-potential clock-bias response.
- **JWST/high-z:** halo-potential response transferred from Cepheid prior.
- **Wide binaries:** weak-field recovery / low-acceleration environmental un-screening.
- **Flyby:** Earth radial screening $S_\oplus(r)$ as local geometric realization of $\mathcal{S}_\Sigma(\mathcal{E})$.
- **LLR:** compactness-dependent Earth/Moon differential screening.
- **LHC:** proximity-saturated hadronic coherence-volume screening.
- **SPIN/QF/KIN:** subatomic proximity/topological-core screening as microscopic projection of $\mathcal{S}_\Sigma(\mathcal{E})$.
- **C0/HC/TH:** temporal-horizon asymptotic transport and late-time conformal acoustic equivalence.

These projections are not interchangeable. Each is calibrated against the environmental variables active in its domain, and evaluating a projection outside the regime where its governing variable dominates yields screening factors that are physically meaningless, as the omitted terms can exceed the retained ones by many orders of magnitude.

The local and cosmological screening responses form a continuous nested hierarchy, not two independent regimes separated by a boundary. The temporal field varies both spatially and temporally: the rate of time differs from place to place, and at any given location it also evolves over time. The cosmological temporal background — the ambient clock-rate field $A(\phi_\infty)$ — is itself spatially varying, with gradients across large-scale structure that can differ substantially between cosmic environments, and temporally evolving, with the cosmological clock rate changing across cosmic history. Within this cosmological baseline, local environmental screening produces additional spatial fluctuations in the observable clock rate and Temporal Shear, smaller in amplitude and varying across shorter scales, and these local fluctuations themselves evolve as the local environment and the cosmological background evolve. The local response is defined relative to the cosmological baseline at the corresponding epoch, not in isolation from it. Both layers are dynamical and continuous in space and time; neither constitutes a discrete transition. The environmental state vector $\mathcal{E}$ therefore carries information at multiple nested scales simultaneously: the cosmological ambient field, the local environmental perturbation, and their coupling, all evaluated at the relevant cosmic epoch. The structure is analogous to temperature in a room: local temperature fluctuates from point to point within the room, but is also defined relative to the external temperature, which itself varies more radically between regions, and all of these temperatures change over time — the room cools at night, the outside temperature shifts with seasons. The temporal field exhibits the same nested character in both dimensions — local clock-rate fluctuations sit within a cosmological time-rate background, both vary continuously across space, and both evolve continuously over time.

The nested structure is quantitative, not merely schematic. Solving the radial field equation for each level of the hierarchy with the containing environment's field as the asymptotic condition — a single continuous profile $\phi_{\text{total}} = \phi_{\text{env}} + \delta\phi$, in which the conformal nonlinearity acts on the total field and the perturbation decays to the ambient value rather than to zero — yields the following decomposition (`step_01_radial_ode`, nested hierarchy). The galactic field at the solar circle is $\phi_{\text{gal}}(8\,\text{kpc}) \simeq 2.8 \times 10^{-7}$ (1.4–5.7×10^{-7} across galactic model variants, consistent with the independent circular-velocity estimate $(v_c/c)^2 \simeq 5.4 \times 10^{-7}$), while the Sun's own perturbation at 1 AU is only 2.0×10^{-8}: the ambient field exceeds the solar contribution beyond $\sim 15\,R_\odot \approx 0.07$ AU, in the $V = 0$ baseline the ambient-to-perturbation ratio is $\sim 9 \times 10^4$ at the wide-binary separation (2646 AU), rising to $\sim 10^7$ in the quartic-screened stellar population — the binary is embedded almost entirely in the galactic field. At the terrestrial surface the decomposition is approximately 93% galactic, 6.5% solar, and 0.5% terrestrial: a local clock measures a small perturbation on a much larger ambient baseline, and because the ambient component is common-mode it cancels in local comparisons. For the same reason the Cassini bound is intrinsically local: it constrains the Sun's gradient perturbation $S_\Sigma^{(\odot)}$, while the ambient galactic field carries negligible gradient over AU scales and drops out of the observable — the nested solution gives $S_\Sigma(1\,\text{AU}) = 1.000279$ versus 1.000280 in isolation for the $V = 0$ baseline, while for the quartic completion ($\mu_0 = 10^5$) the nested and isolated solutions both yield $S_\Sigma(1\,\text{AU}) = 1.46 \times 10^{-3}$ (Cassini-screened in both configurations), leaving the Solar-System verdict unchanged while making its domain of validity precise. The baseline itself is not uniform: the ambient clock rate differs by $\Delta \ln A \simeq 2.2 \times 10^{-7}$ between the solar circle and the galactic halo, so the proper-time field is genuinely position-dependent across the galaxy — one continuous multi-scale profile with no boundaries between levels.

The parameter $\rho_T \approx 20$ g/cm³ is a macroscopic phenomenological saturation scale for the scalar response. It is not a universal microscopic density cutoff, a binary screened/unscreened switch, or automatically applicable to quantum cores without a transfer map. For quantum and accelerator domains, the microscopic topological-core regulator is a proximity/coherence-volume projection of $\mathcal{S}_\Sigma(\mathcal{E})$, not literal bulk density.

Temporal Topology and Temporal Shear: Canonical Formulation

The screening ontology is organized through a sector dictionary. The Temporal Shear is defined as the gradient of the conformal factor:

$$\Sigma_\mu \equiv \nabla_\mu \ln A(\phi) = \frac{\partial \ln A}{\partial \phi} \nabla_\mu \phi = \frac{\alpha(\varphi)}{M_{\rm Pl}} \nabla_\mu \phi, \tag{46}$$

where $\alpha(\varphi) \equiv d(\ln A)/d\varphi$ is the dimensionless conformal coupling strength, and $\varphi \equiv \phi/M_{\rm Pl}$. For compactness one may write $\Theta \equiv \ln A$, but the canonical series notation remains $\ln A$, $\Sigma_\mu = \nabla_\mu \ln A$, and C_A.

The observable Temporal Shear is suppressed by the environmental screening operator $\mathcal{S}_\Sigma(\mathcal{E})$:

$$\Sigma_\mu^{\rm obs} = \mathcal{S}_\Sigma(\mathcal{E})\, \nabla_\mu \ln A(\phi), \tag{47}$$

where the environmental state is

$$\mathcal{E} = \{\rho, \Phi/c^2, \nabla\rho, \nabla\Phi, \text{compactness}, R_T(M), \text{proximity}, T, z, \text{boundary geometry}, \text{coherence volume}\}. \tag{48}$$

The common environmental state $\mathcal{E}$ organizes these domain-specific observable projections; the projections themselves need not be numerically identical.

The Temporal Topology correlation function $C_A(x, x')$ characterizes correlations of conformal-factor fluctuations:

$$C_A(x, x') \equiv \langle \delta \ln A(x)\, \delta \ln A(x') \rangle, \tag{49}$$

It is measured through clock/covariance data.

The temporal correlation length λ_T is the characteristic scale extracted from $C_A(x, x')$ in covariance measurements, not a derived algebraic combination of local fields. The symbols L_c (Papers 6, 10, 23), $L_{\rm macro}$ (Paper 24), $R_T(M_\oplus)$ (Papers 6, 15), and $\lambda_{\rm TEP}$ (Paper 15) are measurement projections of the same scale λ_T, adopted by the corpus as the empirical calibration $L_c \approx 4{,}200$ km from 25-year multi-centre GNSS clock analysis.

The temporal saturation scale ρ_T is the characteristic scale at which Temporal Topology effects saturate in screening; it is a property of the theory's non-linear regime, not a local temporal energy density.

Finally, the observable response of any measurement channel X is parameterized by response coefficients κ_X:

$$\Delta O_X = \kappa_X \cdot \mathcal{S}_X(\mathcal{E}) \cdot \mathcal{F}_X[\Delta \ln A, \Sigma_\mu, C_A; \Phi, \rho, z], \tag{50}$$

where κ_X is an observable response coefficient for channel X, not the microscopic conformal coupling β_A and not a PPN coupling. The locally active PPN coupling is suppressed by the environmental/source screening factor $\mathcal{S}_\Sigma(\mathcal{E})$ and should not be confused with channel response coefficients κ_X.

Universal transfer map ($\beta_A \to \kappa_X$)

The transfer map translates the microscopic coupling $\beta_A = -1.0$ into domain-specific observable response coefficients (κ_X). Channel-specific response coefficients are observable projections of the universal conformal sector, with $\kappa_X = |\beta_A| S_X(\mathcal{E}_X) \Gamma_X$.

They encode the channel geometry and environmental response and are distinct from the frozen microscopic coupling $\beta_A = -1$:

Observable channel coefficients are defined as positive response magnitudes

$$\kappa_X \equiv |\beta_A|\, S_X(\mathcal{E}_X)\, \Gamma_X. \tag{51}$$

They are not the bare coupling. S_X is the screening projection appropriate to the channel: S_A for clock-rate and covariance observables (GNSS, J0437, clock networks), S_Σ for source-charge and fifth-force observables (Cassini, LLR, wide binaries). $\mathcal{E}_X$ is the environmental state evaluated for the target channel. Γ_X is a geometric/kinematic projector that is not tabulated in this paper; it is a known function of the channel geometry.

Domain	Base coupling	Screening projection	Observable response	Status
Solar System / GNSS	$\beta_A = -1.0$	$S_A^{(\oplus)}$ (clock)	λ_T, clock response $\kappa_{\rm GNSS}$	Predicted
Wide binaries	$\beta_A = -1.0$	$S_\Sigma(\rho_{\rm gal\ disk})$	$\alpha_{\rm sat}$	Predicted
Cepheids (H_0)	$\beta_A = -1.0$	$S_A(\rho_{\rm host\ gal})$	$\kappa_{\rm Cep}$	Predicted
JWST high-z	$\beta_A = -1.0$	Stellar-population transfer	$\kappa_{\rm gal}$	Inherited
Globular clusters	$\beta_A = -1.0$	$S_A(\text{cluster env})$	Pulsar Γ	Predicted

By freezing this action, any discrepancy between the predicted κ_X and empirical fits (such as the variation in $\kappa_{\rm Cep}$ between 0.326–0.452 $\times 10^6$ mag and the theory benchmark of 0.96 $\times 10^6$ mag) ceases to be an unconstrained liability and becomes a direct constraint on the kinetic structure of the action.

On the benchmark value and its unit. The canonical figure $\kappa_{\rm canonical} = 0.96 \times 10^6$ mag is a prespecified theory benchmark, not a fitted parameter: it is declared in advance so that downstream analyses (for example the JWST application, Paper 12) can be run without any domain-specific refitting, which is what makes those applications tests rather than fits. The unit "mag" is a bookkeeping convention inherited from the Cepheid period–luminosity relation in which the coefficient was first expressed; in the transfer-map sense of the equation above, κ_X is a dimensionless response magnitude, and the magnitude unit simply records the observational channel through which it is measured. It should not be treated as a physical dimension carried by the coupling.

PPN mapping

In unscreened regimes, the PPN parameter is $\gamma_{\rm PPN} - 1 = -2\alpha_{\rm eff}^2/(1+\alpha_{\rm eff}^2) \simeq -2\alpha_{\rm eff}^2$ for $|\alpha_{\rm eff}| \ll 1$, where $\alpha_{\rm eff} = S_\Sigma\, \alpha_0$ is the screened effective scalar charge. With $\alpha_0 = \beta_A = -1$, Cassini's $|\gamma_{\rm PPN} - 1| < 2.3 \times 10^{-5}$ requires $S_\Sigma^{(\odot)} \lesssim 3.4 \times 10^{-3}$ in the Solar-System environment. Near massive bodies, the suppression of Temporal Shear (vanishing field gradient) suppresses the effective scalar charge to $\alpha_{\rm eff} = S_\Sigma\, \alpha_0 \ll \alpha_0$, cleanly preserving PPN bounds without invoking rigid thin-shell approximations.

PPN recovery in the screened limit. For $A(\phi) = \exp(\beta_A \phi / M_{\rm Pl})$, the dimensionless microscopic coupling is $\alpha_0 \equiv d \ln A / d\varphi = \beta_A = -1$. Environmental screening does not alter this universal microscopic coupling. Instead, it suppresses the effective exterior scalar charge,

$$\alpha_{\rm eff} = S_\Sigma(\mathcal{E})\, \alpha_0, \tag{52}$$

where $S_\Sigma(\mathcal{E}) \to 0$ in dense environments. In the DEF normalization used here,

$$\gamma_{\rm PPN} - 1 = -\frac{2\alpha_{\rm eff}^2}{1+\alpha_{\rm eff}^2}. \tag{53}$$

Therefore $S_\Sigma \to 0 \implies \alpha_{\rm eff} \to 0 \implies \gamma_{\rm PPN} \to 1$. The remaining PPN parameters likewise recover their GR values in the screened limit. No independent running of the frozen microscopic coupling α_0 is required.

Equivalence principle

TEP ensures universality in the matter frame. In the Einstein frame, the apparent fifth force is bounded by Eötvös experiments; MICROSCOPE gives $\eta \lesssim 10^{-14}$. Sectoral dilaton-like couplings (to α, μ, quark masses) are constrained to $|d| \lesssim 10^{-5}$–10^{-6} by composition tests and clock ratios.

Disformal constraints

GW170817/GRB170817A constrain $|c_\gamma - c_g|/c \lesssim \text{few} \times 10^{-15}$ at $z \approx 0.01$, bounding the observable combination $B(\phi)(\partial\phi)^2$ along the observed astrophysical path. This does not require B to vanish identically. In regimes where common-mode conformal effects dominate, B may remain active as a source for synchronization holonomy, multipath propagation anomalies, or interferometric signatures without violating the same-path EM–GW timing bound.

Disformal holonomy and the screening ontology

As established in Section 3.3, the invariant synchronization observable is the GR-subtracted residual

$$H_{\text{resid}}(C) = \oint_C \Delta\sigma, \qquad \Delta\sigma \equiv \tilde{\sigma} - \sigma_{\text{GR}}. \tag{54}$$

In the conformal-only subclass, the scalar clock-rate contribution is the exact one-form $d \ln A$, so it cannot by itself generate closed-loop residual synchronization holonomy in a smooth simply connected region. A leading-order nonzero H_{resid} requires residual synchronization curvature,

$$d\Delta\sigma \neq 0. \tag{55}$$

In the minimal TEP model this curvature is supplied by the disformal sector; in more general extensions it may arise from non-metricity or other explicitly non-exact transport structure.

To state the disformal contribution in a measurement-defined way, let u^μ denote the four-velocity field of the physical clock network or observer congruence used to define the synchronization protocol. The $(-+++)$ signature is used, so that

$$u^\mu u_\mu = -1. \tag{56}$$

Let

$$P_\mu{}^\nu = \delta_\mu{}^\nu + u_\mu u^\nu \tag{57}$$

be the spatial projector into the local rest space of that congruence. To leading order in the disformal correction, the projected contribution to the synchronization connection has the representative form

$$\delta\tilde{\sigma}_\mu \simeq -\frac{B}{A^2}(u \cdot \nabla\phi) P_\mu{}^\nu \nabla_\nu \phi, \tag{58}$$

up to the sign convention used for the synchronization one-form and higher-order disformal corrections.

Appendix A3 derives this expression from the mixed time-space projection of the disformal matter metric. It also shows that synchronization re-gaugings shift both the matter-frame synchronization connection and the corresponding GR reference connection by the same exact one-form. Therefore the GR-subtracted residual connection $\Delta\sigma$ is invariant under synchronization convention changes, and

$$H_{\mathrm{resid}}(C) = \oint_C \Delta\sigma \tag{59}$$

is independent of the arbitrary simultaneity convention used to coordinatize the specified physical clock network.

The invariant claim is therefore precise: H_{resid} is not independent of which physical clock network is used, but for a specified physical clock-network protocol it is independent of arbitrary synchronization re-labelling.

For a hypersurface-orthogonal clock network, $u^\mu = n^\mu$, the projected expression reduces to the familiar $3+1$ form

$$\delta\tilde{\sigma}_i \approx -\frac{B}{A^2 N}(\partial_i\phi)(n\cdot\partial\phi), \tag{60}$$

where N is the lapse and n^μ is the unit normal to the spatial slices. This ADM expression should be read as a special-case representation of the physical congruence formulation, not as the definition of the observable.

Unlike $d\ln A$, the disformal contribution is not generically exact. In the local non-topological case, its curvature satisfies

$$d(\delta\tilde{\sigma}) \neq 0 \tag{61}$$

whenever the prefactor multiplying the projected scalar gradient varies independently around the loop, for example through time dependence, anisotropic boundary conditions, inhomogeneous field structure, lapse/shift structure, or spatial variation of the disformal response within a fixed physical clock-network protocol. For a loop C bounding a smooth surface Σ, the local non-exact contribution to the residual holonomy may be written

$$H_{\mathrm{resid}}(C) = \oint_C \Delta\sigma = \iint_\Sigma d(\Delta\sigma). \tag{62}$$

At leading order beyond the GR-subtracted reference model, $d(\Delta\sigma)$ contains the disformal curvature $d(\delta\tilde{\sigma})$. Topological holonomy, where the loop does not bound a smooth surface or the connection is locally closed but not globally exact, is a separate case and is not represented by the Stokes expression above.

The conformal and disformal responses arise from the same environment-dependent scalar configuration. For the universal exponential coupling,

$$\Sigma_\mu \equiv \nabla_\mu \ln A = \frac{\beta_A}{M_{\mathrm{Pl}}}\nabla_\mu\phi, \tag{63}$$

while the leading disformal deformation relative to the conformal metric is

$$\mathcal{D}_{\mu\nu} \equiv \frac{B(\phi)}{A^2(\phi)}\nabla_\mu\phi\nabla_\nu\phi = \frac{B(\phi)\,M_{\mathrm{Pl}}^2}{A^2(\phi)\,\beta_A^2}\,\Sigma_\mu\Sigma_\nu. \tag{64}$$

Environmental flattening of the Temporal Topology therefore suppresses both responses: Temporal Shear is linear in the locally active scalar gradient, whereas the leading disformal deformation is quadratic in that gradient for fixed B/A^2. Their observable suppression is nevertheless not represented by a single universal numerical factor, because the disformal response additionally depends on $B(\phi)$, the solved field profile, path geometry, boundary conditions, and the observer congruence. The body-level exterior source-charge factor

$$S_\Sigma \equiv Q/Q_0 \tag{65}$$

is an integrated observable projection of the field configuration and should not be inserted directly as a universal local S_Σ^2 multiplier for disformal observables. At leading disformal order, the synchronization correction may equivalently be written

$$\delta\tilde{\sigma}_\mu \simeq -\frac{B(\phi)\, M_{\rm Pl}^2}{A^2(\phi)\, \beta_A^2}\,(u\cdot\Sigma)\, P_\mu{}^\nu \Sigma_\nu. \tag{66}$$

Thus synchronization holonomy depends on the local field value and Temporal Shear, the observer motion relative to that field, the orientation of the gradient, and the complete path geometry. Experimental response therefore cannot in general be inferred from ambient density or a body-level source-charge factor alone.

Accordingly, high-energy, mesoscopic, and topological probes should not be modeled solely by the ambient bulk-density screening function used in astrophysical applications. Their responses are represented by channel-specific coefficients κ_X, depending on momentum transfer, interaction topology, boundary geometry, and microscopic field structure. These probes test whether non-exact disformal transport remains measurable in regimes where the conformal clock-rate response is screened.

8. Cosmology: Static Spatial Geometry, Temporal Horizon, and EFT Mapping

Background & The Temporal Horizon

Supersession Note: Earlier formulations of TEP utilized phenomenological epoch-screening functions to artificially preserve a standard hot-plasma expansion history. The framework now develops thermodynamic closure natively within the canonical eternal-universe architecture. The "hot Big Bang" is formally rejected in the canonical architecture.

The cosmological background is an eternal, static spatial geometry where apparent expansion is reconstructed purely as open-path conformal temporal shear: $1+z = A_0/A_{\rm em}$. The conformal factor changes the operational rate and calibration of matter proper time relative to the static gravitational spatial geometry; TEP does not identify this conformal matter-frame rescaling with physical expansion of the underlying spatial manifold. The apparent spatial singularity conventionally written as $a \to 0$ is formally re-expressed as a regular temporal horizon ($\mathscr{T}^-$) where the observational clock map $A_{\rm clock} \to 0$. In the matter frame, the continuity equation for $\tilde{\rho}_m$ is standard, while apparent kinematic acceleration manifests entirely from the evolving Temporal Shear.

Temporal-Horizon Chemical Equilibrium and Proper-Time Reaction Flow

Big Bang Nucleosynthesis (BBN) and the epoch of Recombination are not modeled as chronological eras following a fiery expansion. Instead, early-universe closure is governed natively by the Proper-Time Reaction Flow over an infinite proper-time history.

The classical stellar astration paradox is resolved natively. While the available proper-time history is unbounded, accumulated stellar processing need not diverge; local chemical evolution can approach a steady-state asymptotic attractor when the temporal-exposure convergence condition is satisfied. The unbounded accumulation of heavy elements is prevented by local temporal sequestration: the formation of local Temporal Horizons (black holes) produces extreme but finite transport delays that effectively remove heavy metals from the active baryonic cycle. Consequently, the observed light-element abundances are not primordial artifacts of a global singularity; rather, TEP-BBN demonstrates a candidate asymptotic chemical attractor in which the observed light-element abundances can arise through long-term baryonic cycling, subject to the temporal-exposure convergence condition derived there.

A candidate TEP origin of the Cosmic Microwave Background is the steady-state thermalization of distributed radiation, with its blackbody form preserved by achromatic conformal transport; TEP-BBN demonstrates this mechanism as a local radiative-transfer proof of concept. The universe becomes completely opaque at high redshift because diverging temporal transport stretches the apparent optical depth to infinity, creating an observable boundary without a physical plasma wall (demonstrated as the 1D Global Opacity Theorem in TEP-BBN). At late times, distance–redshift observables are reconstructed through open-path temporal transport across the inhomogeneous scalar background. Growth and lensing provide independent consistency tests of the realized cosmological solution; their quantitative response must be derived from that solution rather than imposed through a generic unscreened scalar–tensor growth law.

Status of Λ in this framework. The word “illusion” above refers specifically to the phenomenological attribution on the Hubble diagram, and should not be read as a claim that no corresponding energy density exists. Within TEP, Λ is reinterpreted rather than removed: the accelerating-distance signature normally attributed to a cosmological constant is reconstructed as the kinetic energy density of the Temporal Shear field, Ω_ϕ (Papers 18, 26). The observational content of Λ is therefore preserved and re-sourced, not denied. At the level of distance–redshift observables, the temporal-transport description can be degenerate with an expanding-ΛCDM fit on the Hubble diagram (Paper 30). Discrimination therefore requires independent observables, including structure growth, lensing, and clock/transport tests, rather than the distance sector alone.

EFT of dark energy mapping

For comparison with standard cosmological perturbation analyses, the late-time scalar sector can be represented in EFT-of-dark-energy language, with $\alpha_T = 0$ enforcing $c_T = 1$. The braiding and effective Planck-mass-running functions provide a phenomenological dictionary for perturbations of the realized TEP cosmological solution. This mapping does not identify the underlying static spatial manifold with a physically expanding FLRW background; quantitative constraints on the effective functions are developed in the companion cosmology analyses.

Standard sirens

In the late-time conformal limit, EM and GW share null cones; standard siren distances are unaffected kinematically. Subtle, detector time-standard effects may introduce an integrated ϕ-history contribution at the sub-second level over ~100 Mpc; ensemble analyses can bound or detect this.

9. Quantum Clocks, Interferometry, and Composition Dependence

Quantum evolution

Proper-time quantum evolution is defined with respect to matter-frame proper time: $i\hbar d|\psi\rangle/d\tau = \hat{H}|\psi\rangle$, where τ is the proper time defined by the matter metric $\tilde{g}_{\mu\nu}$. Relative to an Einstein-frame or reference coordinate time t, stationary clocks satisfy $d\tau \simeq A(\phi)\,dt$ in the weak field, meaning a single clock's tick rate relative to t carries the $A(\phi)$ scaling. Because this conformal rescaling is locally universal, it cancels exactly from dimensionless ratios of co-located ideal matter clocks. Observable conformal clock signatures arise strictly from comparisons between different spacetime environments, transported clock histories, or small sectoral dilaton-like sensitivities:

$$\delta \ln \nu = \delta \ln A + K_\alpha \delta \ln \alpha + K_\mu \delta \ln \mu + K_q \delta \ln X_q + \dots \tag{67}$$

where the first term represents the universal conformal clock-rate contribution relative to the specified reference standard.

Species sensitivity

For a dimensionless ratio of two co-located clock transitions X and Y, the universal conformal contribution cancels:

$$\delta \ln \frac{\nu_X}{\nu_Y} = (K_{\alpha,X} - K_{\alpha,Y})\delta \ln \alpha + (K_{\mu,X} - K_{\mu,Y})\delta \ln \mu + (K_{q,X} - K_{q,Y})\delta \ln X_q + \dots \tag{68}$$

Multi-species clock comparisons therefore constrain non-universal sectoral couplings, while universal $A(\phi)$ signatures are tested through comparisons of clock rates or accumulated proper-time histories across distinct spacetime environments.

Interferometry

Phases acquire contributions proportional to the integral of $A(\phi)$ along arms. Atom interferometers with vertical baselines can sense $\partial_h \phi$ at 10^{-21}–10^{-22} m^{-1}; photon interferometers are sensitive at different bands.

Decoherence

Rapid ϕ variations would induce dephasing at rates $O(\partial_t \phi)$, strongly bounded by clock stabilities. Adiabatic evolution in the lab is assumed, consistent with null drift bounds.

Inset: What "no-variable-c" tests do—and don't—probe (TEP view)

Gauge-invariant observable. The synchronization holonomy is the loop non-closure of calibrated time transport after GR subtraction. Let σ denote the time-transport one-form whose line integral equals the calibrated proper-time increment along each leg. The residual holonomy is

$$H_{\mathrm{resid}}(C) \equiv \oint_C (\tilde{\sigma} - \sigma_{\mathrm{GR}}) = \iint_\Sigma (\tilde{F} - F_{\mathrm{GR}}), \tag{69}$$

the integral of the residual curvature two-form over a surface Σ bounded by the closed loop $C = \partial\Sigma$. It is built from measured proper-time increments along each leg and has units of time. Because it is the closed-loop integral of the GR-subtracted synchronization connection, $\Delta\sigma = \tilde{\sigma} - \sigma_{\mathrm{GR}}$, it is invariant under admissible synchronization re-gaugings. Re-gaugings shift both the matter-frame connection and the corresponding GR reference connection by the same exact one-form, leaving $\Delta\sigma$ invariant (since $\oint_C d\chi = 0$ for single-valued χ). It vanishes in SR/GR and in the conformal-only limit of TEP. The GR subtraction includes Sagnac, Lense–Thirring/gravito-magnetic, Shapiro, gravitational redshift, station motion, clock-scale realization, and reference-frame corrections, computed with ITRF ephemerides and TT/TDB standards.

How flagship constraints map to H_{resid}:

- **GW170817 (GW–EM coincidence).** $|c_\gamma - c_g|/c \lesssim 10^{-15}$ constrains global cone splits. In TEP, late-time conformal coupling preserves null cones, so EM and GW share causal structure; small disformal tilts today are allowed. This is a boundary condition, not a loop-holonomy test.
- **Cassini (PPN-γ).** Two-way Doppler/Shapiro is reciprocity-even; it calibrates σ_{GR} to subtract but does not bound H_{resid}.
- **Resonator MM/KT tests.** Cavities provide strong terrestrial bounds on even-parity orientation-dependent photon propagation, including the disformal $D(\hat{n} \cdot \nabla\phi)^2$ deformation derived in Appendix B. They do not directly measure the distinct odd/non-exact loop-closure observable H_{resid}, whose leading synchronization kernel additionally depends on observer motion and path geometry.
- **"GPS works."** Network self-consistency uses explicit GR+Sagnac modeling and largely two-way/common-view calibration. This verifies internal consistency under assumed GR model; not a direction-reversing one-way loop-closure null.
- **Clock redshift & pairwise A↔B tests.** Exquisitely confirm GR locally; **only closed loops** (A→B→C→A with direction reversal) can reveal non-integrability captured by H_{resid}.

Why classics can be null while $H_{\mathrm{resid}} \neq 0$:

1. Conformal null-cone invariance ⇒ no large GW–EM kinematic delays (consistent with GW170817).
2. **$\partial_t\phi = 0$ over loop timescale; gradients conservative: no direct conformal propagation asymmetry.** In the purely conformal limit ($B = 0$), the conformal factor cancels exactly from the null condition, so forward/back propagation times are identical. Residuals require the disformal sector, time dependence, or non-exact transport structure. Thus two-way/closed-path nulls can hold while a loop-holonomy test remains sensitive.

Experimental falsifier (primary endpoints). Run a closed-loop, one-way time-transfer (and/or portable-clock) test and report:

- Leg-wise antisymmetry: $\Delta t_{AB} = t_{AB} - t_{BA}$ (and optionally $\Xi_{AB} \equiv (t_{AB} - t_{BA})/(t_{AB} + t_{BA})$).
- Loop holonomy H_{resid} after subtracting the full GR, kinematic, clock-scale, and instrumental synchronization model. Use triangle/quadrilateral geometries with direction reversal; extend with interplanetary one-way links and multi-species clock networks.

10. Experimental Proposals and Falsifiability

A suite of decisive, cross-checking experiments is proposed that can falsify, constrain, or provide controlled support for the theory. All observables are dimensionless ratios or calibrated residuals; all designs include nulls, blinding, and open data.

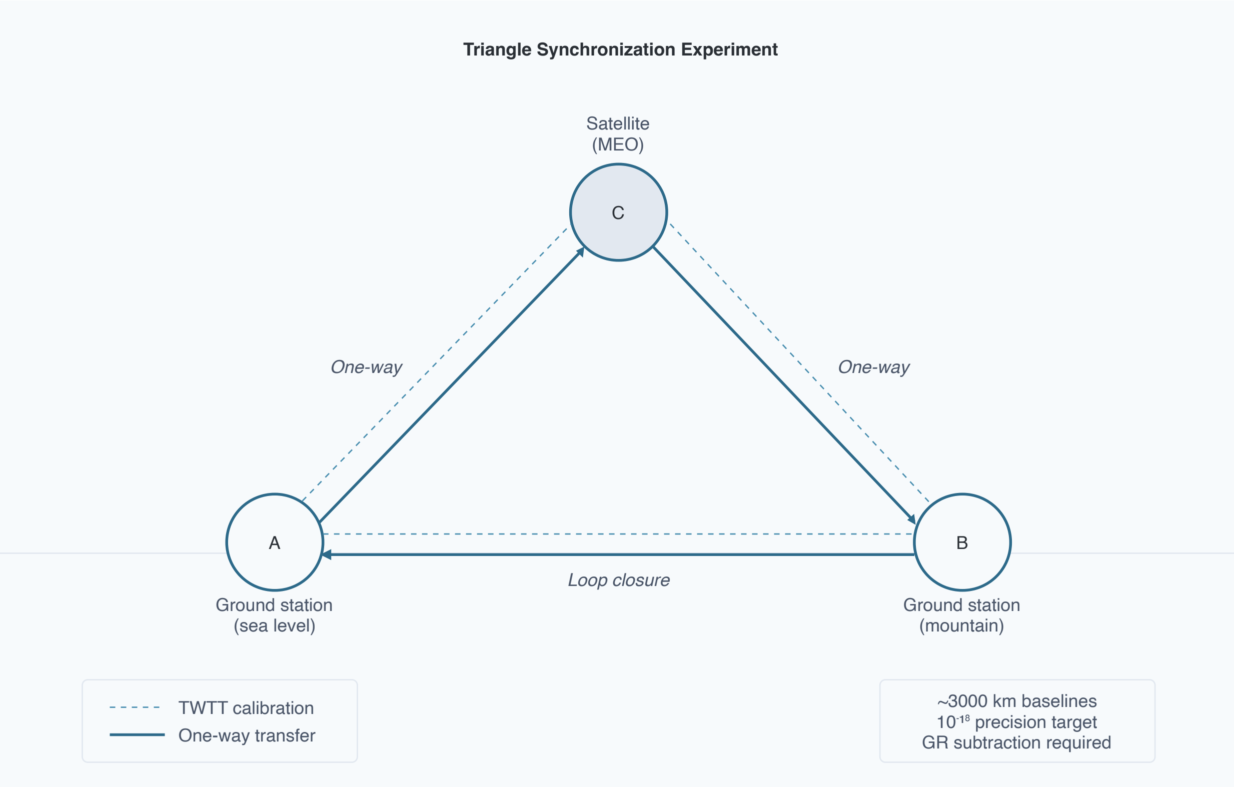

Figure 3. Triangle synchronization experiment geometry. Two ground stations (sea level and mountain) and a medium-Earth-orbit satellite form ~3000 km baselines; two-way time transfer calibrates each edge while one-way transfers around the loop probe H_{resid} after GR subtraction.

A. Triangle synchronization holonomy (ground–ground–satellite)

Geometry. Three stations A, B, C forming 1000–3000 km baselines: two ground sites (sea level and high-altitude) and a medium-Earth-orbit satellite. Optical two-way time transfer (TWTT) on each edge provides calibration; stabilized fibers and free-space optical links carry both calibration and one-way signals.

Protocol. Establish Einstein synchronization on each edge via TWTT. Execute one-way transfers around the loop in both senses at high cadence for months. Record raw timestamps, environmental monitors (pressure, temperature, humidity), refractivity profiles, TEC for ionosphere, and precise ephemerides.

Modeling. Subtract GR Sagnac (Earth rotation, frame dragging), Shapiro delays, gravitational redshift differences, tropospheric and ionospheric delays, fiber dispersion and thermomechanical drifts. Use GNSS and gravimetric models.

Observable. The measured loop residual is

$$H_{\mathrm{resid}}(C) = \oint_C (\tilde{\sigma} - \sigma_{\mathrm{GR}}) = \oint_C \Delta\sigma, \tag{70}$$

where σ_{GR} is computed from the full GR, kinematic, geodetic, atmospheric, instrumental, and clock-scale model for the same loop.

Benchmark sensitivity window. Previous phenomenological estimates motivate sensitivity in the 10^{-18}–10^{-16} fractional range per loop time (0.1–1 s). The absolute TEP signal remains to be derived from the common scalar profile and the disformal synchronization path integral. The ground portion samples the strongly screened near-surface configuration while the space legs probe the radial recovery region; the relative contribution of each segment is therefore a prediction of the completed field solution. The experiment is sensitive to disformal or otherwise non-exact transport contributions. Null in GR by design.

Crucially, while the ground stations (A and B) reside in the near-surface zone where the environmental operator $\mathcal{S}_\Sigma(\mathcal{E})$ heavily suppresses the local temporal shear to satisfy PPN bounds, the space legs traverse the radial altitude gradient $S_\oplus(r)$, rapidly escaping surface screening. The measurable loop holonomy H_{resid} is therefore geometrically sourced by the un-screened vertical segments of the transit, utilizing the heavily screened ground leg primarily as a stable baseline calibration.

```
Error budget (fractional per loop, targets after months):
```

- `Clock instability after averaging:` 5×10^{-19}
- `Two-way calibration residual:` 2×10^{-19}
- `Troposphere residual:` 2×10^{-19}
- `Fiber path noise after stabilization:` 5×10^{-20}
- `Ephemeris/geodesy:` 2×10^{-19}
- `GR subtraction residual:` 5×10^{-19}
- **`Total systematic floor (rss):`** $\sim 8 \times 10^{-19}$

`Target:` `below` 10^{-18}`; projected capability with advanced turbulent cancellation techniques reaches the` 10^{-19} `regime.`

Falsification. Null at the 10^{-18} fractional target across seasons/geometry excludes non-exact transport signatures with late-time cosmological relevance; reaching the projected 10^{-19} capability would extend this exclusion.

B. Portable-clock "clock anholonomy"

Design. Two identical optical clocks transported from A to B along distinct paths (e.g., sea-level highway vs. mountain pass), durations ~1–3 days, then compared at B to a stationary clock. Common-view time transfer provides epoch.

Prediction. Path-dependent discrepancy Δ_{12} at few$\times 10^{-19}$ for plausible $\alpha\dot{\phi}_0$ and $\partial_h\phi$ under screening; null at 10^{-20} bounds $\partial_t\phi$ and $\partial_h\phi$ tightly.

Systematics. Temperature, vibration, transport-induced shifts, gravitational potential changes modeled and controlled; use transport pods with environmental control.

C. Multi-species clock network: annual modulations

Network. Global network of optical clocks (Sr, Yb, Al^+, Hg^+, Ca, H(1s–2s)) cross-compared over years.

Prediction. Phase-locked annual modulations in differential ratios ν_A/ν_B with amplitudes 10^{-19}–10^{-17}, phases tied to orbital eccentricity. Species-amplitude ratios reflect $\alpha_A - \alpha_B$; a fit yields $\alpha(\phi)$ and dilaton coefficients d_e, d_μ, d_q.

Nulls. Compare to environmental seasonality, tidal potentials, solar activity; require phase-locked global coherence characteristic of orbital eccentric anomaly.

D. Interplanetary one-way optical time transfer

Design. Two drag-free spacecraft with 10^{-18}-class optical lattice clocks, separated by 1–5 AU. Optical comb-based one-way time transfer, with third node for calibration (Earth or a relay). Kinematic synchronization via slow-clock transport or common-view transponders.

Benchmark sensitivity window. Geometry-dependent one-way asymmetry parameter $\Xi_{AB} \equiv (t_{AB} - t_{BA})/(t_{AB} + t_{BA})$ at 10^{-15}–10^{-14} (0.05–5 ps) for disformal tilts consistent with GW bounds. The absolute signal magnitude remains to be derived from the solved path-dependent kernel; this range is a benchmark target, not a no-refit prediction.

Systematics. Plasma delays, pointing jitter, thermal drifts, deep-space clock performance; anticipate >decade timeline.

E. Clock Network Correlation Analysis and Environmental Screening Maps

Objective. Detect spatial correlations and environmental screening signatures in atomic clock frequency residuals consistent with screened scalar field coupling $A(\phi)$ to transition frequencies.

Design.
Phase I - Distance Correlation Analysis:
• Analyze existing precision clock networks (GNSS, optical clock arrays) for distance-dependent correlations in frequency residuals
• Apply phase-coherent cross-spectral analysis between station pairs
• Bin pairs by 3D distance, fit exponential correlation model: $C(r) = A \cdot \exp(-r/\lambda_T) + C_0$
• Cross-validate across independent analysis centers to control systematics

Phase II - Environmental Screening Maps:
• Deploy identical optical clocks at sea-level, mountain, stratospheric balloon, and LEO; intercompare with two-way optical links
• Subtract GR redshift and Doppler shifts; correlate residuals with detailed geophysical models and gravimetry to isolate screening signatures

Forecast.
• Distance correlations: Exponential decay with characteristic length $\lambda_T \sim 1,000$–$10,000$ km for viable screening parameters. The empirical terrestrial calibration $L_c \approx 4{,}200$ km, obtained from 25-year multi-centre GNSS clock analysis (Papers 1, 2, 6), falls inside this prespecified theoretical prior. It is an empirical calibration adopted by the corpus, not a value derived here; the held-out MGEX replication (Paper 14) returns a shorter length ($\approx 1{,}400$ km) on a different product type, also within the prespecified theoretical prior. Forward analyses that adopt $\lambda_T \approx 4{,}200$ km should state it as a calibration input.
• Altitude dependence: 10^{-19}–10^{-18} frequency shifts over tens of kilometers for $\lambda_{\text{scr}} \sim 10$ km near Earth

F. Multi-messenger ensemble

Design. Stack $N \gtrsim 30$ multi-messenger events with prompt EM counterparts; marginalize astrophysical lag distributions. Seek distance-correlated trends in $t_{\text{EM}} - t_{\text{GW}}$.

Prediction. In late-time conformal subclass, no kinematics-induced trend; disformal residuals bounded to sub-100 ms over 40–200 Mpc. Nulls constrain $B(\phi_0)(\partial\phi)^2$.

11. Statistical and Open Science Principles

Pre-registration. Publish analysis plans (models, priors, nulls, thresholds) for triangle and portable-clock experiments; record any deviations.

Blinding. Blind event-time stamps and calibration offsets; employ independent teams for calibration and analysis.

Open data/code. Release raw timestamps, environmental monitors, calibration logs, and pipelines with DOIs; release CLASS/HyRec modification, atom-sensitivity database, and meta-analytic code.

Hierarchical inference. Use heavy-tailed likelihoods (Student-t) to mitigate outliers; multi-level random effects by domain; selection models for publication bias; explicit covariance modeling for shared systematics.

12. Addressing Critiques and Clarifying Claims

No EM–GW kinematic delay in conformal subclass. With $B = 0$ today, EM and GW share null cones; any observed delays are astrophysical/source or detector-time-standard effects. Earlier overstatements are corrected and aligned with GW170817 constraints.

Static ϕ gradients do not generate directional propagation asymmetry. The conformal factor cancels from the null condition (Appendix A2), so $A(\phi)$ cannot act as a photon refractive index; clock-rate and open-path redshift effects remain.

Holonomy invariant and not a synchronization artifact. The observable H_{resid} is constructed from physical proper-time measurements as the closed-loop integral of the GR-subtracted synchronization connection, $\Delta\sigma = \tilde{\sigma} - \sigma_{\text{GR}}$. Synchronization re-gaugings shift both the matter-frame connection and the corresponding GR reference connection by the same exact one-form, leaving $\Delta\sigma$ and therefore H_{resid} invariant.

Causality and hyperbolicity. Explicit invertibility and signature conditions are given, restricting to canonical kinetics and small disformal couplings; matter-frame causality is preserved. The small-B regime is safe.

The cosmological implementation has been tested with native hi_class MCMC fits (Paper 18) and Cobaya joint-likelihood analyses (Paper 26), providing evidence that the temporal-horizon architecture respects Planck acoustic anchors while producing late-time environmental observables.

13. Philosophical and Conceptual Implications

Simultaneity beyond Einstein. Special relativity makes simultaneity observer-dependent; dynamic time permits globally non-integrable synchronization through its non-exact transport sector. The invariant content is a holonomy of time transport: moving clocks around closed loops in a dynamical time background returns path-dependent offsets after subtracting GR effects.

Constants clarified. The speed of light is an invariant in local tangent spaces; globally, "c" is not a number but a family of operational ratios dependent on clock histories in a time field. Variation of constants becomes a question about dimensionless ratios across environments and epochs.

Machian undertone. The rate of time responds weakly to the stress-energy of matter through αT, giving a principled, covariant flavor to the idea that the "rest of the universe" influences local rates, without violating local physics.

14. Conclusions

This paper articulates a covariant framework in which the rate of time is a dynamical field with universal matter coupling. The architecture preserves local Lorentz invariance and null-cone structure (in the conformal limit), conforms to multi-messenger bounds, and yields new invariant observables—synchronization holonomy and clock anholonomy—that vanish in GR and are measurable with modern clocks. Screening reconciles local nulls with cosmological dynamics; a controlled disformal sector allows minute, bounded photon-cone tilts that provide clean targets for holonomy experiments. The theory is falsifiable with realistic experiments and promises to clarify persistent cosmological tensions.

Einstein moved us from absolute time to relative simultaneity and dynamic geometry. The next step is to recognize that the flow of time itself is dynamical, and that "the speed of light" is the local echo of a deeper temporal geometry. At weak field, the explicit quartic completion demonstrates that a single density-dependent scalar interaction can satisfy Solar-System source-charge bounds while retaining parsec-scale response in the interstellar medium, providing a concrete cross-scale realization of the Temporal-Topology screening architecture. If the predicted holonomies are observed, physics will enter a new epoch in which dynamic time joins dynamic geometry as a foundation. If not, uniquely strong bounds will have been set and the operational bedrock of c and simultaneity clarified to unprecedented precision.

Appendix A: Proofs and Key Derivations

A1. Conformal null-cone invariance

Let $\tilde{g}_{\mu\nu} = A(\phi)^2 g_{\mu\nu}$ with $A > 0$. A vector k^μ null with respect to $g_{\mu\nu}$, $g_{\mu\nu}k^\mu k^\nu = 0$, satisfies $\tilde{g}_{\mu\nu}k^\mu k^\nu = A^2 g_{\mu\nu}k^\mu k^\nu = 0$. Maxwell's action $S = -(1/4)\int \sqrt{-g}F_{\mu\nu}F^{\mu\nu}$ is conformally invariant in 4D: under $\tilde{g}_{\mu\nu} = \Omega^2 g_{\mu\nu}$, $\sqrt{-\tilde{g}}F_{\mu\nu}F^{\mu\nu} = \sqrt{-g}F_{\mu\nu}F^{\mu\nu}$. Hence photon geodesics are conformally invariant; null cones coincide.

A2. Exact direct conformal propagation null

Consider the purely conformal subclass $\tilde{g}_{\mu\nu} = A^2(\phi)\, g_{\mu\nu}$, $B = 0$. A photon trajectory satisfies

$$\tilde{g}_{\mu\nu}\, k^\mu k^\nu = A^2(\phi)\, g_{\mu\nu}\, k^\mu k^\nu = 0. \tag{71}$$

Because $A(\phi) > 0$, this is equivalent to $g_{\mu\nu}\, k^\mu k^\nu = 0$. Thus the conformal factor does not alter the local null cone or act as a direction-dependent refractive index. In a static conformal background, forward and backward propagation along the same geometrical path therefore acquire no conformal propagation-time antisymmetry:

$$\Delta t^{(A)}_{\text{prop}} \equiv t_\rightarrow - t_\leftarrow = 0. \tag{72}$$

The conformal sector nevertheless remains observable through matter-clock rates and open-path comparisons. For stationary clocks, $d\tilde{\tau} = A(\phi)\, d\tau_g$, so clocks situated in different field environments can acquire different proper-time histories. The corresponding infinitesimal conformal transport is $\omega^{(A)} = d\ln A$, which is exact. Hence, in a smooth simply connected region,

$$\oint_C d\ln A = 0. \tag{73}$$

A static, purely conformal field can therefore produce clock-rate differences and open-path redshift effects, but cannot by itself generate a direction-odd same-path propagation residual or a non-zero closed-loop synchronization holonomy. Such a residual requires the disformal sector $B \neq 0$, explicit time dependence combined with motion through the field, or some other non-exact/topological transport structure.

A3. Synchronization holonomy invariance and projected disformal connection

This appendix derives the leading-order disformal contribution to the synchronization connection used in Section 7 and shows why the GR-subtracted closed-loop residual is invariant under synchronization re-gauging.

A3.1 Synchronization connection and re-gauging

Consider a local threading decomposition of the matter-frame metric relative to a physical clock-network congruence:

$$d\tilde{s}^2 = \tilde{g}_{00}\big(dt + \tilde{\sigma}_i dx^i\big)^2 + \tilde{h}_{ij}dx^i dx^j. \tag{74}$$

Equivalently, up to the sign convention used for $\tilde{\sigma}_i$,

$$\tilde{\sigma}_i = \frac{\tilde{g}_{0i}}{\tilde{g}_{00}}. \tag{75}$$

If the opposite sign convention is adopted, all shifts below acquire the opposite sign, but the closed-loop result is unchanged.

A synchronization re-gauging of the same physical clock network assigns a different simultaneity offset to the same clock worldlines:

$$t' = t + \chi(x^i), \tag{76}$$

where χ is a single-valued spatial clock-offset function on the network at the epoch of the loop measurement. Then

$$dt = dt' - \partial_i \chi \, dx^i. \tag{77}$$

Substituting into the metric gives

$$dt + \tilde{\sigma}_i dx^i = dt' + (\tilde{\sigma}_i - \partial_i \chi) dx^i. \tag{78}$$

Therefore

$$\tilde{\sigma}_i \longrightarrow \tilde{\sigma}'_i = \tilde{\sigma}_i - \partial_i \chi. \tag{79}$$

In one-form notation,

$$\tilde{\sigma} \longrightarrow \tilde{\sigma} - d\chi. \tag{80}$$

With the opposite sign convention for $\tilde{\sigma}$, the sign reverses. In either convention, the change is exact.

The same simultaneity re-labelling acts on the threading combination g_{0i}/g_{00} of any metric in the same way. The GR reference connection σ_{GR} is the corresponding threading connection computed from the GR reference metric on the same physical clock-network congruence, with the same loop, same coordinate convention, and the standard Sagnac, Lense--Thirring, Shapiro, gravitational-redshift, station-motion, clock-scale, and reference-frame corrections included. Therefore the same re-labelling gives

$$\sigma_{\mathrm{GR}} \longrightarrow \sigma_{\mathrm{GR}} - d\chi. \tag{81}$$

The GR-subtracted residual connection

$$\Delta\sigma \equiv \tilde{\sigma} - \sigma_{\mathrm{GR}} \tag{82}$$

therefore transforms as

$$\Delta\sigma \longrightarrow (\tilde{\sigma} - d\chi) - (\sigma_{\mathrm{GR}} - d\chi) = \Delta\sigma. \tag{83}$$

Thus the closed-loop observable

$$H_{\text{resid}}(C) = \oint_C \Delta\sigma \tag{84}$$

is invariant under synchronization re-gauging.

Equivalently, if one works with a representative in which the residual connection itself shifts by an exact form,

$$\Delta\sigma \to \Delta\sigma + d\chi_{\text{res}}, \tag{85}$$

then the loop integral is still invariant because

$$\oint_C d\chi_{\text{res}} = 0 \tag{86}$$

for single-valued χ_{res}. The observable is the loop class of the residual connection modulo exact one-forms, not a raw one-way synchronization convention.

This proof is local in time. The loop C is evaluated on the spatial network at a specified epoch. Time dependence of ϕ, $B(\phi)$, or the matter metric may change the value of $\Delta\sigma$ from one epoch to another, but it does not change the synchronization-gauge argument at a fixed epoch. The gauge freedom relevant to the closed-loop observable is the spatial simultaneity re-labelling $\chi(x^i)$ of the specified physical clock network.

For experimental campaigns extending over months, the integrated data does not evaluate a single 4D spacetime loop, but rather generates a continuous time-series of instantaneous 3D spatial loop integrations, $H_{\text{resid}}(C, t)$. At any given temporal slice t, the spatial simultaneity re-labeling remains strictly exact ($\oint_C d\chi(t, x^i) = 0$). Slow temporal variations in $\phi(t)$, or shifts in the Earth's environmental screening state $\mathcal{E}$ along its orbit, merely manifest as predictable, time-dependent modulations (e.g., annual or diurnal phases) of a continuously gauge-invariant spatial holonomy.

A3.2 Projected disformal contribution

The matter metric is

$$\tilde{g}_{\mu\nu} = A^2(\phi)g_{\mu\nu} + B(\phi)\nabla_\mu\phi\nabla_\nu\phi. \tag{87}$$

Let u^μ be the four-velocity of the physical clock network defining the synchronization protocol, with

$$u^\mu u_\mu = -1 \tag{88}$$

in the $(- + ++)$ signature. The spatial projector into the local rest space of this congruence is

$$P_\mu{}^\nu = \delta_\mu{}^\nu + u_\mu u^\nu. \tag{89}$$

The scalar gradient decomposes as

$$\nabla_\mu\phi = D_\mu\phi - (u \cdot \nabla\phi)u_\mu, \tag{90}$$

where

$$D_\mu \phi = P_\mu{}^\nu \nabla_\nu \phi \tag{91}$$

is the spatial gradient measured by the clock network.

The disformal part of the matter metric is

$$\delta_B \tilde{g}_{\mu\nu} = B \nabla_\mu \phi \nabla_\nu \phi. \tag{92}$$

Its mixed time-space projection relative to the clock-network congruence is

$$P_\mu{}^\alpha u^\beta \delta_B \tilde{g}_{\alpha\beta} = B \left(P_\mu{}^\alpha \nabla_\alpha \phi\right) \left(u^\beta \nabla_\beta \phi\right), \tag{93}$$

so

$$P_\mu{}^\alpha u^\beta \delta_B \tilde{g}_{\alpha\beta} = B D_\mu \phi (u \cdot \nabla \phi). \tag{94}$$

The synchronization connection is the normalized mixed time-space component of the matter metric. In a local rest frame of the clock congruence, the conformal background gives

$$\tilde{g}_{00}^{(A)} = -A^2, \tag{95}$$

while the disformal correction gives

$$\delta_B \tilde{g}_{0i} = B (u \cdot \nabla \phi) D_i \phi. \tag{96}$$

The disformal sector also corrects $\tilde{g}_{00}$ at order $B(u \cdot \nabla\phi)^2$. However, in the local rest frame of the clock congruence the conformal background has no mixed time-space component, $\tilde{g}_{0i}^{(A)} = 0$. Therefore the correction to $1/\tilde{g}_{00}$ multiplies a vanishing conformal numerator and first contributes only at higher order in B. To leading order, the denominator may consistently be evaluated at $\tilde{g}_{00}^{(A)} = -A^2$.

Therefore, to leading order in B, using the convention $\tilde{\sigma}_i = \tilde{g}_{0i}/\tilde{g}_{00}$,

$$\delta \tilde{\sigma}_i \simeq \frac{\delta_B \tilde{g}_{0i}}{\tilde{g}_{00}^{(A)}} \simeq -\frac{B}{A^2} (u \cdot \nabla \phi) D_i \phi. \tag{97}$$

With the opposite convention for the synchronization one-form, the overall sign is reversed; the closed-loop invariance and exact/non-exact distinction are unaffected.

In covariant projected form this is

$$\delta \tilde{\sigma}_\mu \simeq -\frac{B}{A^2} (u \cdot \nabla \phi) D_\mu \phi, \tag{98}$$

or equivalently

$$\delta\tilde{\sigma}_\mu \simeq -\frac{B}{A^2}(u\cdot\nabla\phi)P_\mu{}^\nu\nabla_\nu\phi. \tag{99}$$

Higher-order terms include corrections from the disformal contribution to $\tilde{g}_{00}$, lapse-shift mixing, and higher powers of $B(\nabla\phi)^2/A^2$.

In a hypersurface-orthogonal $3+1$ slicing, where $u^\mu = n^\mu$, this reduces to

$$\delta\tilde{\sigma}_i \approx -\frac{B}{A^2 N}(\partial_i\phi)(n\cdot\partial\phi), \tag{100}$$

up to lapse-shift convention and higher-order disformal corrections.

Furthermore, because the reference connection σ_{GR} is constructed using the exact same non-inertial clock congruence u^μ, any purely kinematic effects arising from the network's proper acceleration or rotation (such as Sagnac or Thomas precession) enter both $\tilde{\sigma}$ and σ_{GR} symmetrically. These kinematics therefore cancel identically in the residual connection $\Delta\sigma = \tilde{\sigma} - \sigma_{\mathrm{GR}}$, ensuring that non-inertial cross-terms do not artificially mimic or contaminate the genuine disformal synchronization holonomy.

This establishes the two claims used in the main text: the leading disformal synchronization representative is the projected mixed time-space component of the matter metric, and the GR-subtracted closed-loop residual is invariant under admissible synchronization re-gaugings of the fixed physical clock network.

A4. Disformal inverse and causality condition

Given $\tilde{g}_{\mu\nu} = A^2 g_{\mu\nu} + B\partial_\mu\phi\partial_\nu\phi$, define the scalar-gradient one-form $q_\mu \equiv \partial_\mu\phi$. The inverse satisfies $\tilde{g}^{\mu\nu}\tilde{g}_{\nu\sigma} = \delta^\mu_\sigma$. Ansätz: $\tilde{g}^{\mu\nu} = A^{-2}(g^{\mu\nu} + Cq^\mu q^\nu)$. Solve for C:

$$A^{-2}[g^{\mu\nu} + Cq^\mu q^\nu][A^2 g_{\nu\sigma} + Bq_\nu q_\sigma] = \delta^\mu_\sigma \tag{101}$$

$$\Rightarrow \delta^\mu_\sigma + A^{-2}(B + A^2 C + BC(q\cdot q))q^\mu q_\sigma = \delta^\mu_\sigma \tag{102}$$

$$\Rightarrow A^2 C + B + BC(q\cdot q) = 0 \Rightarrow C = -\frac{B}{A^2 + B(q\cdot q)}. \tag{103}$$

Thus $\tilde{g}^{\mu\nu} = A^{-2}\left[g^{\mu\nu} - \frac{(B/A^2)q^\mu q^\nu}{1+(B/A^2)(q\cdot q)}\right]$. Lorentzian signature requires $1 + (B/A^2)(q\cdot q) > 0$.

Appendix B: Photon Phase Speed and GW–EM Constraints

In a local inertial frame ($g_{\mu\nu} = \eta_{\mu\nu}$), the photon dispersion relation is $\tilde{g}^{\mu\nu}k_\mu k_\nu = 0$. Using the disformal inverse from A4,

$$\eta^{\mu\nu}k_\mu k_\nu = \frac{(B/A^2)(q\cdot k)^2}{1 + (B/A^2)(q\cdot q)}. \tag{104}$$

For a photon with 4-momentum $k^\mu = (\omega/c,\, k\hat{n})$, where $k \equiv |\vec{k}|$ is not assumed equal to ω/c, and a static scalar gradient $q_\mu = (0, \nabla\phi)$, $q\cdot k = k\,\partial_{\hat{n}}\phi$ and $q\cdot q = |\nabla\phi|^2$. Defining $D \equiv B/A^2$, the dispersion relation gives

$$-\frac{\omega^2}{c^2} + k^2 = \frac{D\,k^2(\partial_{\hat{n}}\phi)^2}{1 + D|\nabla\phi|^2}. \tag{105}$$

Solving for k^2 and extracting the phase speed $v_{\mathrm{ph}} = \omega/k$ yields

$$v_{\rm ph} = c\sqrt{1 - \frac{D(\partial_{\hat n}\phi)^2}{1 + D|\nabla\phi|^2}}. \tag{106}$$

For propagation along the gradient ($\partial_{\hat n}\phi = |\nabla\phi|$), this simplifies to

$$v_\parallel = \frac{c}{\sqrt{1 + D|\nabla\phi|^2}}. \tag{107}$$

For small D, the leading-order result is $v_{\rm ph}/c \simeq 1 - \frac{1}{2}D(\partial_{\hat n}\phi)^2 + \mathcal{O}(D^2)$.

Gravitons propagate on $g_{\mu\nu}$, so $c_g = c$ exactly. The maximal fractional speed difference between photons and gravitons, for propagation perpendicular to $\nabla\phi$ ($\partial_{\hat n}\phi = 0$, $v_\perp = c$) versus along it ($\partial_{\hat n}\phi = |\nabla\phi|$, $v_\parallel = c/\sqrt{1 + D|\nabla\phi|^2}$), is

$$\frac{|c_\gamma - c_g|}{c} = 1 - \frac{1}{\sqrt{1 + D|\nabla\phi|^2}} \approx \frac{D}{2}|\nabla\phi|^2 \quad (\text{for small } D). \tag{108}$$

The GW170817/GRB170817A bound $|c_\gamma - c_g|/c \lesssim \text{few} \times 10^{-15}$ therefore requires

$$D\,|\nabla\phi|^2 = \frac{B(\phi)}{A(\phi)^2}\,|\nabla\phi|^2 \lesssim \text{few} \times 10^{-15} \tag{109}$$

along typical lines of sight today, bounding the present-day disformal coupling $B(\phi_0)$.

Appendix C: Glossary of Symbols

Symbol	Description	Section
$g_{\mu\nu}$	Gravitational metric tensor	2
$\tilde{g}_{\mu\nu}$	Matter/causal metric tensor	2
ϕ	The scalar time field	2
$A(\phi)$	Conformal coupling factor, $\exp(\beta_A \phi / M_{\mathrm{Pl}})$	2
$B(\phi)$	Disformal coupling function	2
TEP	Temporal Equivalence Principle	1, 2
τ	Proper time defined by $\tilde{g}_{\mu\nu}$	2
H_{resid}	residual synchronization holonomy, $H_{\mathrm{resid}}(C) \equiv \oint_C (\tilde{\sigma} - \sigma_{\mathrm{GR}})$	3, 6
$\Delta\sigma$	GR-subtracted synchronization connection, $\Delta\sigma \equiv \tilde{\sigma} - \sigma_{\mathrm{GR}}$	3, 6, 7, A3
u^μ, u_μ	four-velocity field of the physical clock-network congruence (upper index contravariant, lower index covariant)	3, 7, A3
$P_\mu{}^\nu$	spatial projector into the local rest space of the clock-network congruence, $P_\mu{}^\nu = \delta_\mu{}^\nu + u_\mu u^\nu$ in $(-+++)$ signature	7, A3
q_μ	scalar-gradient one-form, $q_\mu \equiv \partial_\mu \phi$	A4, B
c_g, c_γ	Speed of gravity, speed of light (photons)	5
$V(\phi)$	Scalar self-interaction potential; quartic branch provides the explicit weak-field screening completion used here	4
$\alpha(\phi)$	Conformal coupling strength, $d(\ln A)/d\phi$	4
β_A	Dimensionless conformal coupling parameter	2
M	Suppression scale for disformal/EFT operators	4
PPN	Parametrized Post-Newtonian formalism	7
γ_{PPN}, β_{PPN}	Eddington PPN parameters	7
H_0	Hubble constant today	9
S_8	Cosmological parameter for structure growth	9
r_s	Sound horizon at recombination	9
Ξ_{AB}	One-way time asymmetry between A and B	6.4
k^μ	Four-wavevector of a null signal	3.2
$\ln A(\phi)$	conformal factor controlling matter-frame proper time	7
Σ_μ	Temporal Shear vector, $\Sigma_\mu \equiv \nabla_\mu \ln A(\phi)$	7
C_A	covariance of conformal-factor fluctuations, $C_A(x, x') = \langle \delta \ln A(x)\, \delta \ln A(x') \rangle$	7
λ_T	Temporal Topology correlation length measured in clock/covariance data	7
ρ_T	Temporal Topology saturation scale; not a binary ambient-density switch	7
κ_X	Observable response coefficient for channel X, not a microscopic coupling	7

Appendix D: Terminology and Usage Glossary

Canonical Terms

Term	Usage
Temporal Topology	Spatial/covariance structure of the time field ϕ.
Temporal Shear	Active gradient $\Sigma_\mu = \nabla_\mu \ln A(\phi)$.
Screening	Suppression of local observable shear/response by $\mathcal{S}_\Sigma(\mathcal{E})$ (not applicable to global cosmological origins).
Conformal sector	$A(\phi)$, clock rates, open-path transport.
Disformal sector	$B(\phi)$, cone tilts, non-exact transport.
Synchronization holonomy	Closed-loop residual only (H_{resid}).
Clock-network covariance	GNSS/SLR/MGEX-type spatial correlation.
Response coefficient	Observable channel transfer parameter κ_X, distinct from the microscopic coupling.
Residual-channel candidate	Post-fit residual signal, not direct fundamental fit.
Stress test	Mixed/null/diagnostic paper.
Inherited calibration	Parameter imported from earlier paper.
No-refit prediction	External prior applied without tuning.

Sector Consistency Rules

Conformal sector. The conformal sector ($A(\phi)$) governs clock-rate, redshift, open-path, and covariance observables. Because $\nabla_\mu \ln A$ is exact, pure conformal shear does not produce closed-loop residual synchronization holonomy. Holonomy requires disformal or otherwise non-exact transport structure.

Response-coefficient rule. Fitted quantities such as κ_X, Γ_X, α_{sat}, and η_{resid} are observable response parameters. They are not bare scalar couplings unless a solved transfer function is supplied.

Evidence-status rule. Every corpus paper is classified as primary evidence, consistency check, stress test, candidate application, null audit, or theoretical completion. Its result is counted accordingly in the corpus-level evidence ledger.

References

Einstein, A. (1905). Zur Elektrodynamik bewegter Körper. Ann. Phys. 17, 891–921.

Einstein, A. (1916). Die Grundlage der allgemeinen Relativitätstheorie. Ann. Phys. 49, 769–822.

Will, C. M. (2014). The Confrontation between General Relativity and Experiment. Living Rev. Relativity 17, 4.

Bertotti, B., Iess, L. & Tortora, P. (2003). A test of general relativity using radio links with the Cassini spacecraft. Nature 425, 374–376.

Bekenstein, J. D. (1993). The relation between physical and gravitational geometry. Phys. Rev. D 48, 3641.

Damour, T. & Polyakov, A. M. (1994). The string dilaton and a least coupling principle. Nucl. Phys. B 423, 532.

Khoury, J. & Weltman, A. (2004). Chameleon fields: Awaiting surprises for tests of gravity in space. Phys. Rev. Lett. 93, 171104.

Hinterbichler, K. & Khoury, J. (2010). Symmetron fields. Phys. Rev. Lett. 104, 231301.

Abbott, B. P. et al. (LIGO/Virgo) (2017). GW170817: Observation of gravitational waves from a binary neutron star inspiral. Phys. Rev. Lett. 119, 161101.

Abbott, B. P. et al. (2017). Multi-messenger observations of a binary neutron star merger. ApJ 848, L12.

Planck Collaboration (2020). Planck 2018 results. VI. Cosmological parameters. A&A 641, A6.

Riess, A. G. et al. (2022). A comprehensive measurement of the local value of the Hubble constant. ApJ 934, L7.

Bothwell, T. et al. (2022). JILA Sr optical lattice clock with 10−18 stability and accuracy. Nature 602, 420–424.

Touboul, P. et al. (2022). MICROSCOPE mission: test of the equivalence principle in space. Phys. Rev. Lett. 129, 121102.

Burrage, C. & Sakstein, J. (2018). Tests of chameleon gravity. Living Rev. Relativity 21, 1.

Bettoni, D. & Liberati, S. (2013). Disformal invariance of second-order scalar-tensor theories. Phys. Rev. D 88, 084020.

Koivisto, T. S. & Zumalacárregui, T. (2013). Disformal gravity. Phys. Rev. D 88, 084016.

Ashby, N. (2003). Relativity in the Global Positioning System. Living Rev. Relativity 6, 1.

Uzan, J.-P. (2011). Varying constants, gravitation and cosmology. Living Rev. Relativity 14, 2.

Michelson, A. A. & Morley, E. W. (1887). On the relative motion of the Earth and the luminiferous ether. Am. J. Sci. 34, 333–345.

Kennedy, R. J. & Thorndike, E. M. (1932). Experimental establishment of the relativity of time. Phys. Rev. 42, 400–418.

Müller, H. et al. (2003). Modern Michelson-Morley experiment using cryogenic optical resonators. Phys. Rev. Lett. 91, 020401.

Herrmann, S. et al. (2009). Test of the isotropy of the speed of light using a continuously rotating optical resonator. Phys. Rev. Lett. 95, 150401.

IERS Conventions (2010). Gérard Petit and Brian Luzum (eds.). IERS Technical Note No. 36, Frankfurt am Main: Verlag des Bundesamts für Kartographie und Geodäsie.

How to cite

You can cite all versions by using the DOI: 10.5281/zenodo.16921911

BibTeX:

```
@misc{Smawfield_TEP_2025,
  author       = {Matthew Lukin Smawfield},
  title        = {Temporal Equivalence Principle: Dynamic Time &
                  Emergent Light Speed},
  year         = {2025},
  publisher    = {Zenodo},
  doi          = {10.5281/zenodo.16921911},
  url          = {https://doi.org/10.5281/zenodo.16921911},
  note         = {Preprint}
}
```

Contact

For questions, comments, or collaboration opportunities regarding this work, please contact:

Matthew Lukin Smawfield
matthew@mlsmawfield.com